Influence of liquid sloshing on dynamics of flexible space structures

メタデータ	言語: English
	出版者:
	公開日: 2020-09-23
	キーワード (Ja):
	キーワード (En):
	作成者: Chiba, Masakatsu, Magata, Hidetaka
	メールアドレス:
	所属:
URL	http://hdl.handle.net/10466/00017049

Influence of liquid sloshing on dynamics of flexible space structures

M. Chiba[a,*], H. Magata[a]

[a] *Department of Aerospace Engineering, Graduate School of Engineering, Osaka Prefecture University, 1-1 Gakuen-cho, Naka-ku, Sakai, Osaka 599-8531, Japan*

ABSTRACT This study involved an analysis of the influence of liquid sloshing on the dynamics of flexible space structures with liquid on-board by considering the main body of a spacecraft as a rigid tank, the flexible appendages as two elastic beams, and on-board liquid as an ideal liquid. The meniscus of the free surface of the liquid due to surface tension was considered. The Lagrangians of the main body of the spacecraft (rigid tank), liquid, and two beams (flexible appendages) were used in addition to assuming symmetric motion of the system; the frequency equations of the coupled system were obtained by applying the Rayleigh–Ritz method. The influence of sloshing motion on the motions of the main body and flexible appendages of the spacecraft was investigated. The results indicated that the vibration characteristics of the coupled system were dependent on the static contact angle of the liquid, irrespective of whether the angle was larger/smaller than $\theta_0 = 90°$.

1. Introduction

Large space structures vibrate easily at low frequencies because they possess low structural rigidity, given their need to be lightweight. Attitude control or orbit modification through thruster injection could cause flexible appendages such as antennae and solar arrays, as well as the liquid fuel or wastewater on the space station, to vibrate and develop strong coupled vibrations that exert a complex effect on the dynamic behaviour of the main body. This poses a serious problem for high-attitude-accuracy satellites such as those used for precise astronomical photography. Therefore, it is essential to clarify the dynamic interaction behaviour of a flexible space structure with on-board liquid in advance, to improve the stability and reliability of space structures.

Several researchers have examined the sloshing of liquids in containers in low-gravity environments theoretically. For example, in 1966, Abramson conducted a review of studies conducted up until 1966 [1]. Bauer et al. (1990 [2], 1990 [3]) conducted free vibration analyses of a liquid in a cylindrical or rectangular vessel taking into consideration the liquid meniscus due to surface tension. In 1993, Agrawal analysed the dynamic behaviour of liquid in a rotating space vehicle using a boundary-layer model [4]. In 1999, Komatsu investigated theoretically the sloshing frequency in a space vehicle tank using a mechanical model, and used potential flow models to obtain natural frequencies via a semi-empirical formula [5]. In 2002, Chiba et al. investigated the coupled natural vibration of an elastic membrane bottom and liquid in a cylindrical container with a rigid wall [6]. In 2004, Utsumi proposed mechanical models for sloshing in a tear-shaped axisymmetric tank [7]. In 2007, Yuanjun et al. carried out a nonlinear analysis of liquid sloshing in a

cylindrical container

Nomenclature : (non-dimensional)

A	Cross sectional area of beam	$z_0(r)$	Static liquid free surface : $\left(\eta_0 = z_0 / R\right)$
b	Length of tank	$Z(r, \varphi, t)$	Amplitude of liquid surface
E	Young's modulus of beam		: $\left(\zeta = Z / R\right)$
h	Equivalent liquid height	$Z_f(r, \varphi, t)$	Displacement of liquid free surface
	: $\left(h_0 = h / R\right)$	$\Phi(r, \varphi, z, t)$	Liquid velocity potential
l	Second moment of area of beam		: $\left(\phi = \Phi / \omega_b R^2\right)$
l	Length of beam $\left(\lambda = l / R\right)$	θ_0	Static contact angle of liquid
m_f	Mass of liquid : $\left(\bar{m}_f = m_f / 2\rho_b Al\right)$	ρ_f	Density of liquid
m_t	Mass of rigid tank	ρ_b	Density of beam
	: $\left(\bar{m}_t = m_t / 2\rho_b Al\right)$	σ	Coefficient of free surface tension
M	Summation of m_f and m_t		: $\left(\gamma = \sigma R^2 l / EI\right)$
	: $\left(\bar{M} = \bar{m}_f + \bar{m}_t\right)$	$\bar{\beta}$	Area ratio of beam and tank $\left(= \pi R^2 / 2A\right)$
o $- XY$	Coordinate system for spacecraft	$\bar{\rho}$	Density ratio $\left(= \rho_f / \rho_b\right)$
o $- r\varphi z$	Coordinate system for tank	ω_b	Natural circular frequency of beam
	: $\left(\text{o} - \rho\varphi\eta\right)$		$\left(= \sqrt{EI / \rho_b Al^4}\right)$
R	Radius of rigid tank	ξ_i	Non-dimensional coordinate : $\left(= x_i / l\right)$
t	Time : $\left(\tau = \omega_b t\right)$	ω	Coupled natural circular frequency
Y_M	Displacement of rigid tank		$\left(\Omega = \omega / \omega_b\right)$
	: $\left(y_M = Y_M / l\right)$		
$W_i(x_i, t)$	Displacements of beams		
	: $\left(w_i = W_i / l\right)$		

considering the static meniscus shape in low-gravity environments using an energy method under pitching excitation around the centre of gravity of the cylinder [8]. In 2007, Berglund et al. controlled the sloshing of liquid propellant in a Delta IV rocket using a pulse-suppression approach [9].

However, only a few experimental studies have focused on resolving the sloshing that occurs in low-gravity environments. In 2005, the Netherlands Agency for Aerospace, NIVR, launched a 130 kg miniature satellite called "Sloshsat Flevo" with an 87 l tank, with 33.5 l of water, to investigate the effect of sloshing behaviour on the motion of the satellite [10].

Additionally, with respect to the effects of sloshing on spacecraft motion, McIntyre et al. in 1982 revealed the relationship between the balance and stability of a flat, rotating spacecraft with liquid fuel on-board [11]. Santini et al. in 1978 and 1983 analysed the influence of motion around the centre of gravity on sloshing in orbital space structures through force balance, and discussed its stability [12, 13]. Jing et al., in 2005, analysed the vibration due to liquid motion in a rectangular tank with flexible appendages subjected to pitching excitation using the energy method under conditions of microgravity and gravity [14]. Buzhinskii, in 2009, studied the effect of sloshing on rocket motion and modelled it as a thin-walled structure with liquid [15]. Recently, Farhat et al., in 2013, investigated the effect of fuel sloshing on a spacecraft and its flutter

characteristics [16].

A recent study constituted the initial step in clarifying the fundamental vibration characteristics of flexible space structures with on-board liquid by proposing a mechanical model, and theoretically analysing the axisymmetric coupled vibrations of a flexible structure with on-board liquid in zero-gravity environments [17]. The proposed model involved modelling the main body as a rigid mass, flexible appendages as two elastic beams, and on-board liquid as a "spring-mass" system (mechanical model). A single liquid sloshing mode (i.e. fundamental sloshing mode) was adopted in the mechanical model, and this helped in determining the fundamental vibration characteristics of the coupled system, i.e. the main body-flexible appendages-liquid system. The present study follows on from the aforementioned study as the second step, and includes a fluid model in which the liquid is modelled as an ideal liquid considering the meniscus due to surface tension.

2. Basic equations and boundary conditions

2.1. Analytical model

In the study, the free vibrations of a spacecraft in space were considered as shown in Fig. 1. The spacecraft included flexible appendages, such as solar arrays on both sides of the main body, and the liquid on-board. The main body of the spacecraft was modelled as a rigid tank, the flexible appendages as two elastic beams, and the on-board liquid as an ideal liquid.

A rigid cylindrical tank with radius R and length b has a mass m_t and a displacement represented by Y_M in the inertia coordinate $\mathrm{o} - XY$.

The beams were modelled as uniform Euler–Bernoulli beams with length l, cross-sectional area A, density ρ_b, Young's modulus E, second moment of area I, and displacements corresponding to $W_1(x_1,t)$ and $W_2(x_2,t)$. The on-board liquid was treated as an inviscid ideal-liquid with density ρ_f and mass $m_f = \pi R^2 h \rho_f$, where h denoted liquid height when the meniscus of the liquid is ignored. The velocity potential of the liquid $\Phi(r,\varphi,z,t)$ is introduced in the coordinate system $\mathrm{o} - rz\varphi$ in which the origin is considered to be located on a flat liquid surface. In a zero-gravity condition, the surface tension was predominant on the liquid that produced an axisymmetric meniscus $z_0(r)$ as shown in Fig. 1(b) with contact angle θ_0 with respect to a side wall. Therefore, the free surface of the liquid is represented as $Z_f(r,\varphi,t) = z_0(r) + Z(r,\varphi,t)$.

It was assumed that the two beams were arranged symmetrically with respect to the rigid tank, and that the mass centre of the rigid tank was located on the mid-surface of the beams. This enabled axisymmetric in-plane motion, i.e. movement along only the upward and downward directions in the plane of the figure.

2.2. Basic equations and boundary conditions for liquid

It is assumed that the liquid is incompressible, inviscid, and exhibits irrotational motion, based on which there exists velocity potential of the liquid $\Phi(r,\varphi,z,t)$ that satisfies the Laplace equation as follows:

$$\Delta \Phi = \frac{\partial^2 \Phi}{\partial r^2} + \frac{1}{r}\frac{\partial^2 \Phi}{\partial \varphi^2} + \frac{\partial^2 \Phi}{\partial z^2} = 0 \tag{1}$$

The free surface of the liquid represents the meniscus $z_0(r)$ due to surface tension and vibrates with a small amplitude $Z(r,\varphi,t)$ around its equilibrium state; thus, the kinematic condition must be satisfied on the free surface as follows:

$$\frac{\partial \Phi}{\partial z} - \frac{\partial Z}{\partial t} - \frac{\partial \Phi}{\partial r}\left[\frac{\partial Z}{\partial r} + \frac{\partial z_0(r)}{\partial r}\right] - \frac{1}{r^2}\frac{\partial \Phi}{\partial \varphi}\frac{\partial Z}{\partial \varphi} = 0 \qquad at \ z = z_0(r) + Z(r,\varphi,t) \tag{2}$$

It is assumed that the motion is axisymmetric and has a small amplitude, and thus Eq. (2) reduces to the following expression:

$$\frac{\partial \Phi}{\partial z} - \frac{\partial Z}{\partial t} - \frac{\partial z_0(r)}{\partial r}\frac{\partial \Phi}{\partial r} = 0 \qquad at \ z = z_0(r) \tag{3}$$

However, the dynamic condition on the free surface is obtained from the Bernoulli equation as follows:

$$\frac{\partial \Phi}{\partial t} + \frac{1}{2}\left(\nabla \Phi\right)^2 + \frac{\sigma}{\rho_f}\left\{\left(\frac{1}{R_1} + \frac{1}{R_2}\right) - \frac{2\cos\theta_0}{R}\right\} = -\ddot{Y}_M(t)z \qquad at \ z = z_0(r) + Z(r,\varphi,t) \qquad (4)$$

where R_1 and R_2 denote the mean curvatures, and the dot represents the derivative with respect to time. The right-hand side of Eq. (4) represents the inertial force due to the motion of the main body (tank). Bauer et al. introduced the following relationship on the curvature shown in Eq. (4) [2]:

$$\frac{1}{R_1} + \frac{1}{R_2} = \frac{-2\cos\theta_0}{R} - \frac{1}{r}\frac{\partial}{\partial r}\left\{ r\left[1 - \left(\frac{r\cos\theta_0}{R}\right)^2\right]^{\frac{3}{2}}\frac{\partial Z}{\partial r}\right\} - \frac{1}{r^2}\sqrt{1 - \left(\frac{r\cos\theta_0}{R}\right)^2}\frac{\partial^2 Z}{\partial \varphi^2} \qquad (5)$$

Based on Eq. (4), Eq. (5), and the above assumptions, the following expression was obtained:

$$\rho_f \frac{\partial \Phi}{\partial t} - \frac{\sigma}{r}\frac{\partial}{\partial r}\left[r\left\{1 - \left(\frac{r\cos\theta_0}{R}\right)^2\right\}^{\frac{3}{2}}\frac{\partial Z}{\partial r}\right] = -\rho_f \ddot{Y}_M(t)z \qquad at \ z = z_0(r) \qquad (6)$$

where the dot represents the derivative with respect to time.

In the analysis, it is assumed that the bottom and side walls of the tank are rigid; thus it is necessary to satisfy the velocity matching conditions at the bottom and on the side walls as follows:

$$\frac{\partial \Phi}{\partial z} = 0 \qquad at \ z = -h \qquad (7)$$

$$\frac{\partial \Phi}{\partial r} = 0 \qquad at \ r = R \qquad (8)$$

Additionally, it is assumed that the contact angle did not change as given in the following expression:

$$\frac{\partial Z}{\partial r} = 0 \qquad at \ r = R \qquad (9)$$

The conservation of liquid volume is represented as follows:

$$\int_0^{2\pi}\int_0^R Z(r,\varphi,t)\,r\,dr\,d\varphi = 0 \qquad (10)$$

The meniscus of the free surface of the liquid caused by surface tension is represented by Bauer et al. [2] as a function of the contact angle θ_0 with respect to the side walls of the tank using the following expression:

$$z_0(r) = \frac{2R\left(1 - \sin^3\theta_0\right)}{3\cos^3\theta_0} - \frac{R}{\cos\theta_0}\sqrt{1 - \left(\frac{r\cos\theta_0}{R}\right)^2} \qquad (11)$$

2.3. Boundary conditions of elastic beams

The elastic beams that represent the solar array paddles, or antennae, were modelled as beams with a "mass-free" boundary condition, i.e. the mass is half of the sum of the tank mass m_t, and liquid mass m_f is expressed as follows: $(M = m_t + m_f)/2$. At the mass-attached end, the shearing force of the beam was balanced with the inertia force of mass $M/2$, and the deflection angle was zero. At the free edge, the shearing force and the bending moment are zero and expressed as follows [17]:

5

$$-\frac{1}{2}M\ddot{Y}_M(t) - EI\frac{\partial^3 W_i(x_i,t)}{\partial x_i^3} = 0, \qquad \frac{\partial W_i(x_i,t)}{\partial x_i} = 0 \qquad at \quad x_i = 0$$

$$-EI\frac{\partial^2 W_i(x_i,t)}{\partial x_i^2} = 0, \qquad -EI\frac{\partial^3 W_i(x_i,t)}{\partial x_i^3} = 0 \qquad at \quad x_i = l \tag{12}$$

2.4. Lagrangian

The Lagrangian of the liquid, beams and the main body (tank) are now considered.

2.4.1. Lagrangian of liquid

The Lagrangian of liquid L_f is represented as a summation of the kinetic energy of the liquid due to rigid tank motions and the dynamic term that was introduced by Luke [18] as follows:

$$L_f = \frac{1}{2}m_f\dot{Y}_f^2 + \int_0^R\int_0^{2\pi}\left\{\rho_f\frac{\partial\Phi}{\partial t} - \frac{\sigma}{r}\frac{\partial}{\partial r}\left[r\left\{1-\left(\frac{r\cos\theta_0}{R}\right)^2\right\}^{3/2}\frac{\partial Z}{\partial r}\right] + \rho_f\ddot{Y}_M(t)z\right\}Zr\,dr\,d\varphi \tag{13}$$

$$at \quad z = z_0(r)$$

2.4.2. Lagrangian of beams and the main body (tank)

The Lagrangian of the beams and the main body (tank) comprise kinetic energy T and potential energy U, and is expressed as follows [17]:

$$\begin{aligned}
L_{tb} &= T - U\\
&= \frac{1}{2}m_t\dot{Y}_M^2 + \frac{\rho_b A}{2}\int_0^l\dot{W}_1^2(x_1,t)dx_1 + \frac{\rho_b A}{2}\int_0^l\dot{W}_2^2(x_2,t)dx_2\\
&\quad -\frac{EI}{2}\int_0^l\left(\frac{\partial^2 W_1(x_1,t)}{\partial x_1^2}\right)^2 dx_1 - \frac{EI}{2}\int_0^l\left(\frac{\partial^2 W_2(x_2,t)}{\partial x_2^2}\right)^2 dx_2
\end{aligned} \tag{14}$$

2.4.3. Non-dimensionalisation

This includes the introduction of the following non-dimensional parameters as given below:

$$\tau = \omega_b t, \omega_b = \sqrt{\frac{EI}{\rho_b A l^4}}, \xi_i = \frac{x_i}{l}, w_i = \frac{W_i}{l}, y_M = \frac{Y_M}{l}, \Omega = \frac{\omega}{\omega_b}, \phi = \frac{\Phi}{\omega_b R^2}$$

$$\rho = \frac{r}{R}, \eta = \frac{z}{R}, \eta_0 = \frac{z_0}{R}, \zeta = \frac{Z}{R}, h_0 = \frac{h}{R}, \bar{\beta} = \frac{\pi R^2}{2A}, \lambda = \frac{l}{R}, \bar{\rho} = \frac{\rho_f}{\rho_b} \tag{15}$$

$$\gamma = \frac{\sigma Al}{EI}, \bar{m}_t = \frac{m_t}{2\rho_b Al}, \bar{m}_f = \frac{m_f}{2\rho_b Al} = \frac{\bar{\rho}\bar{\beta}h_0}{\lambda}, \bar{M} = \bar{m}_t + \bar{m}_f$$

In the above parameters, tank mass ratio $\bar{M}$, sectional area ratio of the beam and the main body (tank) $\bar{\beta}$, ratio of length of the elastic beam and tank radius λ, surface tension parameter γ, liquid height ratio h_0,

and density ratio $\bar{\rho}$ are important parameters.

Non-dimensionalised equations for liquid

The non-dimensional forms of Eq. (1), Eq. (3), and Eq. (6) to Eq. (11). in which the dot represents the derivative with non-dimensional time τ. are as follows:

$$\Delta\phi = 0 \tag{1'}$$

$$\frac{\partial\phi}{\partial\eta} - \frac{\partial\zeta}{\partial\tau} - \frac{\partial\eta_0(\rho)}{\partial\rho}\frac{\partial\phi}{\partial\rho} = 0 \qquad at \quad \eta = \eta_0(\rho) \tag{3'}$$

$$\frac{\partial\phi}{\partial\tau} - \frac{\lambda^3\gamma}{\bar{\rho}}\frac{1}{\rho}\frac{\partial}{\partial\rho}\left[\rho\left\{1 - (\rho\cos\theta_0)^2\right\}^{3/2}\frac{\partial\zeta}{\partial\rho}\right] = -\lambda\ddot{y}_M\eta_0 \tag{6'}$$

$$\frac{\partial\phi}{\partial\eta} = 0 \qquad at \quad \eta = -h_0 \tag{7'}$$

$$\frac{\partial\phi}{\partial\rho} = 0 \qquad at \quad \rho = 1 \tag{8'}$$

$$\frac{\partial\zeta}{\partial\rho} = 0 \qquad at \quad \rho = 1 \tag{9'}$$

$$\int_0^{2\pi}\int_0^1 \zeta(\rho,\varphi,\tau)\rho\,d\rho\,d\varphi = 0 \tag{10'}$$

$$\eta_0(\rho) = \frac{2(1-\sin^3\theta_0)}{\cos^3\theta_0} - \frac{1}{\cos\theta_0}\sqrt{1-(\rho\cos\theta_0)^2} \tag{11'}$$

The non-dimensional form of beam boundary conditions is represented as follows:

$$-\bar{M}\ddot{y}_M - \frac{\partial^3 w_i(\xi_i,\tau)}{\partial\xi_i^3} = 0, \quad \frac{\partial w_i(\xi_i,\tau)}{\partial\xi_i} = 0 \qquad at \quad \xi_i = 0$$

$$\frac{\partial^2 w_i(\xi_i,\tau)}{\partial\xi_i^2} = 0, \qquad \frac{\partial^3 w_i(\xi_i,\tau)}{\partial\xi_i^3} = 0 \qquad at \quad \xi_i = 1 \tag{12'}$$

Non-dimensional form of Lagrangian for liquid

The non-dimensional Lagrangian of Eq. (13) is represented as $\bar{L}_f = L_f\lambda^2 / \rho_b Al^3\omega_b^2$.

$$\bar{L}_f = \lambda^2\bar{m}_f\dot{y}_M^2 + \frac{2\bar{\beta}\bar{\rho}}{\pi\lambda}\int_0^1\int_0^{2\pi}\left\{\frac{\partial\phi}{\partial\tau} - \frac{\lambda^3\gamma}{\bar{\rho}}\frac{1}{\rho}\frac{\partial}{\partial\rho}\left[\rho\left\{1-(\cos\theta_0)^2\right\}^{3/2}\frac{\partial\zeta}{\partial\rho}\right] + \lambda\ddot{y}_M\eta_0\right\}\zeta\rho\,d\rho\,d\varphi$$
$$at \quad \eta = \eta_0(\rho) \tag{13'}$$

The non-dimensional form of the Lagrangian for beams and rigid tank is as follows:

$$\overline{L}_{tb} = \lambda^2 \overline{m}_t \dot{y}_M^2 + \frac{1}{2}\lambda^2 \int_0^1 \dot{w}_1^2 d\xi_1 + \frac{1}{2}\lambda^2 \int_0^1 \dot{w}_2^2 d\xi_2 - \frac{\lambda^2}{2}\int_0^1 \left(\frac{\partial^2 w_1}{\partial \xi_1^2}\right)^2 d\xi_1 - \frac{\lambda^2}{2}\int_0^1 \left(\frac{\partial^2 w_2}{\partial \xi_2^2}\right)^2 d\xi_2 \qquad (14)'$$

3. Method of solution

3.1. Elimination of temporal terms

It is assumed that the system undergoes small-amplitude harmonic motion with circular frequency Ω as follows:

$$\begin{aligned}
y_M(\tau) &= \overline{y}_M \cos\Omega\tau \\
\phi(\rho,\eta,\tau) &= -\Omega\overline{\phi}(\rho,\eta)\sin\Omega\tau \\
\zeta(\rho,\tau) &= \overline{\zeta}(\rho)\cos\Omega\tau \\
w_i(\xi_i,\tau) &= \overline{w}_i(\xi_i)\cos\Omega\tau \quad (i=1,2)
\end{aligned} \qquad (16)$$

Substituting Eq. (16) into the Lagrangian for the liquid in Eq. (13)' and integrating for a period of vibration $\tau = 0 \sim 2\pi/\Omega$ and $\tilde{L}_f = \dfrac{\Omega}{\pi}\displaystyle\int_0^{2\pi/\Omega} \overline{L}_f d\tau$ gives the following expression:

$$\tilde{L}_f = \lambda^2 \overline{m}_f \Omega^2 \overline{y}_M^2 - \frac{2\overline{\beta}\overline{\rho}}{\pi\lambda}\int_0^1\int_0^{2\pi}\left\{\Omega^2\overline{\phi} + \frac{\lambda^3\gamma}{\overline{\rho}}\frac{1}{\rho}\frac{\partial}{\partial\rho}\left[\rho\left\{1-\left(\rho\cos\theta_0\right)^2\right\}^{3/2}\frac{\partial\overline{\zeta}}{\partial\rho}\right] + \lambda\Omega^2\overline{y}_M\eta_0\right\}\overline{\zeta}\rho\, d\rho\, d\varphi \qquad (13)''$$

$$at \quad \eta = \eta_0(\rho)$$

In the above integrations, the following formula is used:

$$\int_0^{2\pi/\Omega}\sin^2\Omega\tau\, d\tau = \int_0^{2\pi/\Omega}\cos^2\Omega\tau\, d\tau = \frac{\pi}{\Omega}$$

Similarly, from the Lagrangians for the beams and the main body (tank), the following expression is obtained:

$$\begin{aligned}
\tilde{L}_{tb} &= \lambda^2 \overline{m}_t \Omega^2 \overline{y}_M^2 + \frac{1}{2}\lambda^2\Omega^2\int_0^1 \overline{w}_1^2(\xi_1)d\xi_1 + \frac{1}{2}\lambda^2\Omega^2\int_0^1 \overline{w}_2^2(\xi_2)d\xi_2 \\
&\quad - \frac{\lambda^2}{2}\int_0^1\left(\frac{\partial^2\overline{w}_1}{\partial\xi_1^2}\right)^2 d\xi_1 - \frac{\lambda^2}{2}\int_0^1\left(\frac{\partial^2\overline{w}_2}{\partial\xi_2^2}\right)^2 d\xi_2
\end{aligned} \qquad (14)''$$

3.2. Lagrangian for liquid

The liquid velocity potential that satisfies Laplace equation (1)' and the boundary conditions in Eq. (3)', Eq. (6) to Eq. (9)', and the displacement of a free surface are assumed in the following form:

$$\begin{aligned}
\overline{\phi}(\rho,\eta) &= \sum_d A_{0d} J_0(\varepsilon_{0d}\rho)\frac{\cosh\left[\left(\varepsilon_{0d}(\eta+h_0)\right)\right]}{\cosh(\varepsilon_{0d}h_0)} \\
\overline{\zeta}(\rho) &= \sum_e a_{0e} J_0(\varepsilon_{0e}\rho)
\end{aligned} \qquad (17)$$

where $J_0(\varepsilon_{0e}\rho)$ denotes the zeroth order Bessel function of the first kind, and ε_{0d} denotes parameters that satisfy $J_0'(\varepsilon_{0d})\left(=-J_1(\varepsilon_{0d})\right) = 0$.

Substituting Eq. (17) into the Lagrangian $\tilde{L}_f$ in Eq. (13)" results in the following expression:

$$\tilde{L}_f = \lambda^2 \bar{m}_f \Omega^2 \bar{y}_M^2 - \frac{2\bar{\beta}\bar{\rho}}{\pi\lambda} \int_0^1 \int_0^{2\pi} \Bigg\{ \Omega^2 \sum_d A_{0d} J_0(\varepsilon_{0d}\rho) \frac{\cosh\left[\varepsilon_{0d}(\eta_0(\rho)+h_0)\right]}{\cosh(\varepsilon_{0d}h_0)}$$

$$+ \frac{\lambda^3\gamma}{\bar{\rho}} \frac{1}{\rho}\frac{\partial}{\partial\rho}\left[\rho\left(1-(\rho\cos\theta_0)^2\right)^{3/2} \sum_e a_{0e}\varepsilon_{0e}J_0'(\varepsilon_{0e}\rho)\right] + \lambda\Omega^2\bar{y}_M\eta_0(\rho)\Bigg\} \sum_e a_{0e}J_0(\varepsilon_{0e}\rho)\rho\,d\rho\,d\varphi \tag{18}$$

Here, the three terms in $\{\ \}$ in the above equation are expanded in the Dini series as follows:

$$\tilde{L}_f = \lambda^2 \bar{m}_f \Omega^2 \bar{y}_M^2$$

$$- \frac{2\bar{\beta}\bar{\rho}}{\pi\lambda} \int_0^1 \int_0^{2\pi} \left[\begin{array}{l} \sum_i \left\{ \Omega^2 \sum_d A_{0d} C_{1di} J_0(\varepsilon_{0i}\rho) + \frac{\lambda^3\gamma}{\bar{\rho}} \sum_e a_{0e} C_{2ei} J_0(\varepsilon_{0i}\rho) + \lambda\Omega^2\bar{y}_M C_{3i} J_0(\varepsilon_{0i}\rho) \right\} \\ \times \sum_n a_{0n} J_0(\varepsilon_{0n}\rho) \end{array} \right] \rho\,d\rho\,d\varphi \tag{19}$$

where

$$C_{1di} = \frac{2}{J_0^2(\varepsilon_{0i})} \int_0^1 \frac{\cosh\left[\varepsilon_{0d}(\eta_0(\rho)+h_0)\right]}{\cosh(\varepsilon_{0d}h_0)} J_0(\varepsilon_{0d}\rho) J_0(\varepsilon_{0i}\rho)\rho\,d\rho$$

$$C_{2ei} = \frac{2}{J_0^2(\varepsilon_{0i})} \varepsilon_{0e} \int_0^1 \frac{1}{\rho}\frac{\partial}{\partial\rho}\left[\rho\left\{1-(\rho\cos\theta_0)^2\right\}^{3/2} J_0'(\varepsilon_{0e}\rho)\right] J_0(\varepsilon_{0i}\rho)\rho\,d\rho$$

$$= -\frac{2}{J_0^2(\varepsilon_{0i})} \varepsilon_{0i}\varepsilon_{0e} \int_0^1 \left\{1-(\rho\cos\theta_0)^2\right\}^{3/2} J_0'(\varepsilon_{0e}\rho) J_0'(\varepsilon_{0i}\rho)\rho\,d\rho \tag{20}$$

$$C_{3i} = \frac{2}{J_0^2(\varepsilon_{0i})} \int_0^1 \eta_0(\rho) J_0(\varepsilon_{0i}\rho)\rho\,d\rho$$

Integrating Eq. (19) with respect to ρ and φ results in the following equation for the Lagrangian:

$$\tilde{L}_f = \lambda^2 \bar{m}_f \Omega^2 \bar{y}_M^2 - \frac{2\bar{\beta}\bar{\rho}}{\lambda} \sum_i a_{0i} J_0^2(\varepsilon_{0i})\left[\Omega^2 \sum_d A_{0d} C_{1di} + \frac{\lambda^3\gamma}{\bar{\rho}} \sum_e a_{0e} C_{2ei} + \lambda\Omega^2\bar{y}_M C_{3i} \right] \tag{21}$$

In the calculation, the orthogonality of the Bessel function is used as follows:

$$\int_0^1 J_0(\varepsilon_{0e}\rho) J_0(\varepsilon_{0i}\rho)\rho\,d\rho = \frac{J_0^2(\varepsilon_{0i})}{2}\delta_{ei}, \tag{22}$$

where δ_{in} denotes the Kronecker delta.

This is followed by substituting Eq. (16) and Eq. (17) into the kinematic condition on the free surface as shown in Eq. (3)', and using Eq. (22) to obtain the following expression:

$$\frac{2}{J_0^2(\varepsilon_{0n})} \sum_d A_{0d}\varepsilon_{0d} \int_0^1 \frac{\sinh\left[\varepsilon_{0d}(\eta_0(\rho)+h_0)\right]}{\cosh(\varepsilon_{0d}h_0)} J_0(\varepsilon_{0d}\rho) J_0(\varepsilon_{0n}\rho)\rho\,d\rho - a_{0n}$$

$$- \frac{2}{J_0^2(\varepsilon_{0n})} \sum_d A_{0d}\varepsilon_{0d} \int_0^1 \frac{\rho\cos\theta_0}{\sqrt{1-(\rho\cos\theta_0)^2}} \frac{\cosh\left[\varepsilon_{0d}(\eta_0(\rho)+h_0)\right]}{\cosh(\varepsilon_{0d}h_0)} J_0'(\varepsilon_{0e}\rho) J_0(\varepsilon_{0n}\rho)\rho\,d\rho = 0$$

$$\frac{\partial\bar{\phi}(\rho,\eta)}{\partial\eta} - \bar{\zeta}(\rho) - \frac{\partial\eta_0(\rho)}{\partial\rho}\frac{\partial\bar{\phi}(\rho,\eta)}{\partial\rho} = 0 \qquad \text{at } \eta = \eta_0(\rho) \tag{3"}$$

Finally, a_{0n} can be represented in terms of A_{0d} as follows:

$$a_{0n} = \sum_d A_{0d}\varepsilon_{0d}C_{4dn} - \sum_d A_{0d}\varepsilon_{0d}C_{5dn}$$

$$= \sum_d A_{0d}\varepsilon_{0d}\left(C_{4dn} - C_{5dn}\right) \tag{23}$$

where

$$C_{4dn} = \frac{2}{J_0^2(\varepsilon_{0n})}\int_0^1 \frac{\sinh\left[\varepsilon_{0d}\left(\eta_0(\rho)+h_0\right)\right]}{\cosh(\varepsilon_{0d}h_0)}J_0(\varepsilon_{0d}\rho)J_0(\varepsilon_{0n}\rho)\rho d\rho$$

$$C_{5dn} = \frac{2}{J_0^2(\varepsilon_{0n})}\int_0^1 \frac{\rho\cos\theta_0}{\sqrt{1-(\rho\cos\theta_0)^2}}\frac{\cosh\left[\varepsilon_{0d}\left(\eta_0(\rho)+h_0\right)\right]}{\cosh(\varepsilon_{0d}h_0)}J_0'(\varepsilon_{0d}\rho)J_0(\varepsilon_{0n}\rho)\rho d\rho \tag{24}$$

By using Eq. (23), the Lagrangian in Eq. (21) for the liquid is obtained as follows:

$$\tilde{L}_f = \lambda^2 \bar{m}_f \Omega^2 \bar{y}_M^2$$

$$-\frac{2\bar{\beta}\bar{\rho}}{\lambda}\sum_i J_0^2(\varepsilon_{0i})\sum_j A_{0j}\varepsilon_{0j}\left(C_{4ji}-C_{5ji}\right)\left[\sum_d A_{0d}\left\{\Omega^2 C_{1di} + \frac{\lambda^3\gamma}{\bar{\rho}}\sum_e \varepsilon_{0d}\left(C_{4de}-C_{5de}\right)C_{2ei}\right\} + \lambda\Omega^2\bar{y}_M C_{3i}\right] \tag{25}$$

3.3. Lagrangian for the beams and the main body (tank)

Substituting Eq. (16) into the boundary conditions in Eq. (12) results in the following expression:

$$\bar{M}\Omega^2\bar{y}_M + \frac{\partial^3\bar{w}_i(\xi_i)}{\partial\xi_i^3} = 0, \qquad \frac{\partial\bar{w}_i(\xi_i)}{\partial\xi_i} = 0 \qquad at \quad \xi_i = 0$$

$$\frac{\partial^2\bar{w}_i(\xi_i)}{\partial\xi_i^2} = 0, \qquad \frac{\partial^3\bar{w}_i(\xi_i)}{\partial\xi_i^3} = 0 \qquad at \quad \xi_i = 1 \tag{12"}$$

Here, the beam displacements are represented as follows:

$$\bar{w}_1(\xi_1) = \sum_m B_m \tilde{w}_{1m}(\xi_1), \qquad \bar{w}_2(\xi_2) = \sum_m C_m \tilde{w}_{2m}(\xi_2), \tag{26}$$

where B_m and C_m denote unknown constants, and $\tilde{w}_{im}(\xi_i):i=1,2$ denotes the eigenfunctions of the beam that satisfy the boundary conditions in Eq. (12)": i.e. mass-free [17].

The Lagrangian for the beams and the main body (tank) is then obtained using Eq. (14)" as follows:

$$\tilde{L}_{tb} = \lambda^2\bar{m}_t\Omega^2\bar{y}_M^2$$

$$+\frac{1}{2}\lambda^2\Omega^2\sum_m\sum_n B_m B_n\int_0^1 \tilde{w}_{1m}(\xi_1)\tilde{w}_{1n}(\xi_1)d\xi_1 + \frac{1}{2}\lambda^2\Omega^2\sum_m\sum_n C_m C_n\int_0^1 \tilde{w}_{2m}(\xi_1)\tilde{w}_{2n}(\xi_2)d\xi_2$$

$$-\frac{\lambda^2}{2}\sum_m\sum_n B_m B_n\int_0^1 \tilde{w}_{1m}''(\xi_1)\tilde{w}_{1n}''(\xi_1)d\xi_1 - \frac{\lambda^2}{2}\sum_m\sum_n C_m C_n\int_0^1 \tilde{w}_{2m}''(\xi_2)\tilde{w}_{2n}''(\xi_2)d\xi_2 \tag{27}$$

Here, the two beams have identical geometrical and material properties, thus $B_m = C_m$. resulting in the following expression:

$$\tilde{L}_{tb} = \lambda^2\left\{\bar{m}_t\Omega^2\bar{y}_M^2 + \Omega^2\sum_m\sum_n B_m B_n X_{mn}^{00} - \sum_m\sum_n B_m B_n X_{mn}^{22}\right\} \tag{28}$$

10

3.4. Lagrangian for the entire system

Finally, the Lagrangian for the entire system is obtained as follows:

$$\tilde{L} = \tilde{L}_f + \tilde{L}_{tb}$$

$$= \lambda^2 \left\{ \bar{m}_f \Omega^2 \bar{y}_M^2 + \bar{m}_t \Omega^2 \bar{y}_M^2 + \Omega^2 \sum_m \sum_n B_m B_n X_{mn}^{00} - \sum_m \sum_n B_m B_n X_{mn}^{22} \right\}$$

$$- \frac{2\bar{\beta}\bar{\rho}}{\lambda} \sum_i J_0^2 (\varepsilon_{0i}) \sum_j A_{0j} \varepsilon_{0j} \left(C_{4ji} - C_{5ji} \right) \tag{29}$$

$$\times \left[\sum_d A_{0d} \left\{ \Omega^2 C_{1di} + \frac{\lambda^3 \gamma}{\bar{\rho}} \sum_e \varepsilon_{0d} \left(C_{4de} - C_{5de} \right) C_{2ei} \right\} + \lambda \Omega^2 \bar{y}_M C_{3i} \right]$$

Here, it is necessary for the displacement of the beam root end and that of the main body (tank) to be equal, as follows:

$$\bar{y}_M = \bar{w}_i(0) = \sum_m B_m \tilde{w}_{im}(0) \tag{30}$$

Given this, $\bar{y}_M$ can be represented in terms of B_m and $\tilde{L}$ as follows:

$$\tilde{L} = \tilde{L}_f + \tilde{L}_{tb}$$

$$= \lambda^2 \left(\bar{m}_f + \bar{m}_t \right) \Omega^2 \sum_m \sum_n B_m B_n \tilde{w}_{1m}(0) \tilde{w}_{1n}(0) + \lambda^2 \Omega^2 \sum_m \sum_n B_m B_n X_{mn}^{00} - \lambda^2 \sum_m \sum_n B_m B_n X_{mn}^{22}$$

$$- \frac{2\bar{\beta}\bar{\rho}}{\lambda} \sum_i J_0^2 (\varepsilon_{0i}) \sum_j A_{0j} \varepsilon_{0j} \left(C_{4ji} - C_{5ji} \right) \tag{31}$$

$$\times \left[\sum_d A_{0d} \left\{ \Omega^2 C_{1di} + \frac{\lambda^3 \gamma}{\bar{\rho}} \sum_e \varepsilon_{0d} \left(C_{4de} - C_{5de} \right) C_{2ei} \right\} + \lambda \Omega^2 \sum_m B_m \tilde{w}_{1m}(0) C_{3i} \right]$$

$$\tilde{\tilde{L}} = \tilde{L} / \lambda^2$$

$$= -\sum_m \sum_n X_{mn}^{22} B_m B_n + \Omega^2 \sum_m \sum_n \left\{ \left(\bar{m}_f + \bar{m}_t \right) \tilde{w}_{1m}(0) \tilde{w}_{1n}(0) + X_{mn}^{00} \right\} B_m B_n$$

$$- 2\bar{\beta}\gamma \sum_j \sum_d A_{0j} A_{0d} \varepsilon_{0j} \varepsilon_{0d} \sum_i \sum_e J_0^2 (\varepsilon_{0i}) C_{2ei} \left(C_{4de} - C_{5de} \right) \left(C_{4ji} - C_{5ji} \right)$$

$$- \frac{2\bar{\beta}\bar{\rho}}{\lambda^3} \Omega^2 \sum_j \sum_d A_{0j} A_{0d} \varepsilon_{0j} \sum_i J_0^2 (\varepsilon_{0i}) C_{1di} \left(C_{4ji} - C_{5ji} \right) \tag{32}$$

$$- \frac{2\bar{\beta}\bar{\rho}}{\lambda^2} \Omega^2 \sum_j \sum_m A_{0j} B_m \varepsilon_{0j} \tilde{w}_{1m}(0) \sum_i J_0^2 (\varepsilon_{0i}) \left(C_{4ji} - C_{5ji} \right) C_{3i}$$

Hence, as indicated by the above discussion, the Lagrangian $\tilde{\tilde{L}}$ can be represented in terms of A_{oj} and B_m.

3.5. Rayleigh–Ritz method

The Rayleigh–Ritz method is applied here to obtain the following minimalised condition for $\tilde{\tilde{L}}$:

$$\frac{\partial \tilde{\tilde{L}}}{\partial A_{0j}} = 0, \quad \frac{\partial \tilde{\tilde{L}}}{\partial B_m} = 0 \tag{33}$$

$$
\frac{\partial \tilde{\tilde{L}}}{\partial A_{0j}} = -2\bar{\beta}\gamma \sum_d A_{0d} \{\varepsilon_{0j}\varepsilon_{0d} \sum_i \sum_e J_0^2(\varepsilon_{0i}) C_{2ei} \left(C_{4de} - C_{5de}\right)\left(C_{4ji} - C_{5ji}\right)
$$
$$
+ \varepsilon_{0d}\varepsilon_{0j} \sum_i \sum_e J_0^2(\varepsilon_{0i}) C_{2ei} \left(C_{4je} - C_{5je}\right)\left(C_{4di} - C_{5di}\right)\}
$$
$$
- \frac{2\bar{\beta}\bar{\rho}}{\lambda^3}\Omega^2 \sum_d A_{0d} \{\varepsilon_{0j} \sum_i J_0^2(\varepsilon_{0i}) C_{1di} \left(C_{4ji} - C_{5ji}\right) + \varepsilon_{0d} \sum_i J_0^2(\varepsilon_{0i}) C_{1ji} \left(C_{4di} - C_{5di}\right)\}
$$
$$
- \frac{2\bar{\beta}\bar{\rho}}{\lambda^2}\Omega^2 \varepsilon_{0j} \sum_m B_m \tilde{w}_{1m}(0) \sum_i J_0^2(\varepsilon_{0i})\left(C_{4ji} - C_{5ji}\right) C_{3i} = 0
$$

$$
-\bar{\beta}\gamma \sum_d A_{0d}\varepsilon_{0j}\varepsilon_{0d} \sum_i \sum_e J_0^2(\varepsilon_{0i}) C_{2ei} \{\left(C_{4de} - C_{5de}\right)\left(C_{4ji} - C_{5ji}\right) + \left(C_{4je} - C_{5je}\right)\left(C_{4di} - C_{5di}\right)\}
$$
$$
- \frac{\bar{\beta}\bar{\rho}}{\lambda^3}\Omega^2 \sum_d A_{0d} \sum_i J_0^2(\varepsilon_{0i})\{\varepsilon_{0j}C_{1di}\left(C_{4ji} - C_{5ji}\right) + \varepsilon_{0d}C_{1ji}\left(C_{4di} - C_{5di}\right)\} \tag{34}
$$
$$
- \frac{\bar{\beta}\bar{\rho}}{\lambda^2}\Omega^2 \varepsilon_{0j} \sum_m B_m \tilde{w}_{1m}(0) \sum_i J_0^2(\varepsilon_{0i})\left(C_{4ji} - C_{5ji}\right) C_{3i} = 0
$$

$$
\frac{\partial \tilde{\tilde{L}}}{\partial B_m} = -2\sum_n X_{mn}^{22} B_n + 2\Omega^2 \sum_n \{ \left(\bar{m}_f + \bar{m}_t\right)\tilde{w}_{1m}(0)\tilde{w}_{1n}(0) + X_{mn}^{00} \} B_n
$$
$$
- \frac{2\bar{\beta}\bar{\rho}}{\lambda^2}\Omega^2 \tilde{w}_{1m}(0) \sum_j \sum_i A_{0j}\varepsilon_{0j} J_0^2(\varepsilon_{0i})\left(C_{4ji} - C_{5ji}\right) C_{3i} = 0
$$

$$
-\sum_n X_{mn}^{22} B_n + \Omega^2 \sum_n \{ \left(\bar{m}_f + \bar{m}_t\right)\tilde{w}_{1m}(0)\tilde{w}_{1n}(0) + X_{mn}^{00} \} B_n
$$
$$
- \frac{\bar{\beta}\bar{\rho}}{\lambda^2}\Omega^2 \tilde{w}_{1m}(0) \sum_j \sum_i A_{0j}\varepsilon_{0j} J_0^2(\varepsilon_{0i})\left(C_{4ji} - C_{5ji}\right) C_{3i} = 0 \tag{35}
$$

The above equations can be represented in the following matrix form as coupled equations in terms of A_{0d} and B_m. Thus, the problem can be reduced into an eigenvalue problem from which the coupled natural circular frequencies can be obtained as eigenvalues, and the vibration modes as eigenvectors in the following manner:

$$\left[\mathbf{K} - \Omega^2 \mathbf{M}\right]\begin{Bmatrix} \mathbf{B} \\ \mathbf{A} \end{Bmatrix} = \mathbf{0}, \tag{36}$$

where

$$\mathbf{K} = \begin{bmatrix} \bar{\mathbf{X}}^{22} & \mathbf{0} \\ \mathbf{0} & \mathbf{D} \end{bmatrix}, \quad \mathbf{M} = \begin{bmatrix} \bar{\mathbf{X}}^{00} & \mathbf{F}^T \\ \mathbf{F} & \mathbf{G} \end{bmatrix}, \quad \mathbf{B} = \{B_m\}^T, \text{ and } \mathbf{A} = \{A_{0d}\}^T,$$

12

$$D_{jd} = -\bar{\beta}\gamma\varepsilon_{0j}\varepsilon_{0d}\sum_i\sum_e J_0^2(\varepsilon_{0i})C_{2ei}\left\{(C_{4de}-C_{5de})(C_{4ji}-C_{5ji})+(C_{4je}-C_{5je})(C_{4di}-C_{5di})\right\},$$

$$\bar{X}_{nm}^{22} = -X_{nm}^{22},$$

$$G_{jd} = \frac{\bar{\beta}\bar{\rho}}{\lambda^3}\sum_i J_0^2\left(\varepsilon_{0i}\right)\left\{\varepsilon_{0j}(C_{4ji}-C_{5ji})C_{1di}+\varepsilon_{0d}(C_{4di}-C_{5di})C_{1ji}\right\},$$

$$F_{jm} = \frac{\bar{\beta}\bar{\rho}}{\lambda^2}\sum_i J_0^2\left(\varepsilon_{0i}\right)\varepsilon_{0j}(C_{4ji}-C_{5ji})C_{3i}\tilde{w}_{1m}(0),$$

and $\bar{X}_{nm}^{00} = -\left(\bar{m}_f+\bar{m}_t\right)\tilde{w}_{1m}(0)\tilde{w}_{1n}(0)-X_{nm}^{00}.$

$$\left(d=1,2,\cdots l,\quad j=1,2,\cdots l,\quad n=1,2,\cdots k,\quad m=1,2,\cdots k\right)$$

(37)

4. Numerical results

A goal of this study included clarifying the influence of liquid-sloshing on the coupled hydroelastic vibration characteristics of the flexible space structure. This involved a step-by-step procedure beginning with determining the static meniscus of the liquid in a cylindrical tank, followed by treating the sloshing characteristics in both an anchored cylindrical tank and a freely floating cylindrical tank, and finally proceeding to a system tank with a beam and without a liquid.

The effective range of system parameters, i.e. $\bar{m}_t, \bar{\rho}, \gamma, \bar{\beta}, \lambda$, etc. is shown in Appendix A. In the numerical calculations, the unknown parameters A_{0d} and B_m in Eq. (36) included five terms for each parameter to satisfy the requirements for engineering data.

4.1. Meniscus of free surface

Meniscus shapes of the free surface for contact angles $\theta_0 = 0°, 30°, \cdots, 180°$ are shown in Fig. 2 based on Eq. (11)' [2]. The liquid surface was flat for $\theta_0 = 90°$, concave for $\theta_0 < 90°$, and convex for $90° < \theta_0$. It was assumed that the liquid surface vibrated around this meniscus shape with a small amplitude.

4.2. Sloshing characteristics in an anchored tank without beam

It is important to approximate the vibration characteristics of a liquid in an anchored cylindrical tank to compare with those of the coupled system floating in space, as shown later. In this case, the frequency equation was obtained by omitting the displacements of beams, i.e. $\boldsymbol{B}$ in Eq. (36), and the system parameters in this case corresponded to θ_0, h_0, $\bar{\rho}$, γ, and λ, with $\lambda = 1$, and the other four parameters were varied.

Variations of the natural circular frequencies up to the third mode with contact angle θ_0 are shown in Fig. 3(a) when $h_0 = 1, \gamma = 1 \times 10^{-6}$, and $\bar{\rho} = 1$. The maximum natural circular frequency occurred at $\theta_0 = 90°$, and it decreased with either increases or decreases in θ_0, which was the same as the results obtained by Bauer et al. [2].

Variations in the natural circular frequencies with liquid height h_0 are shown in Fig. 3(b), when $\theta_0 = 90^0, \gamma = 1 \times 10^{-6}$, and $\bar{\rho} = 1$, in which the natural circular frequency increased with h_0 and converged to a constant value representing the same tendency as that in a tank on earth.

Next, Fig. 3(c) represents the influence of the surface tension parameter γ on the natural circular frequency when $h_0 = 1, \theta_0 = 90^0$, and $\bar{\rho} = 1$, while Fig. 3(d) represents the influence of density ratio $\bar{\rho}$ when $h_0 = 1$, $\theta_0 = 90^0$, and $\gamma = 1 \times 10^{-6}$.

Finally, the variations of the vibration mode with contact angle θ_0 are shown in Fig. 4, when $h_0 = 1$, $\gamma = 1 \times 10^{-6}$, and $\bar{\rho} = 1$. In the figures, the meniscus shapes are denoted using dashed lines, and the vibration modes are normalized as maximum amplitudes to be unity. The influence of the contact angle θ_0 can be seen in the displacement near the side wall.

4.3. Sloshing characteristics in a tank floating in space

This section discusses a spacecraft floating in space when the beams are rigid, which corresponds to the system in which the solar paddles are undeveloped. In this case, the system parameters include γ, h_0, λ,

θ_0, $\bar{\beta}$, $\bar{\rho}$, $\bar{m}_t$ and $\bar{m}_f$. It was assumed that $\bar{\beta} = 10$ and $\lambda = 1$.

4.3.1. Influence of contact angle

Figure 5 shows the variations of natural circular frequencies up to the third mode with contact angle θ_0 when $h_0 = 1$, $\gamma = 1 \times 10^{-6}$, $\bar{\rho} = 1$, and $\bar{m}_t = 10$. In this figure, solid lines represent the results in a floating tank, and dotted lines those in an anchored tank that corresponds to Fig. 3(a), with the former being only slightly higher than the latter. Additionally, even by changing $\bar{m}_t$ from 1 to 100, no influence of the tank mass ratio $\bar{m}_t$ on the natural frequency was observed.

4.3.2. Influence of contact angle on vibration mode

Vibration modes were obtained using the same parameters as shown in Fig. 4 when $\bar{m}_t = 10$, $\lambda = 1$, and $\bar{\beta} = 10$, but the results were almost the same as Fig. 4 and thus are omitted here.

4.3.3. Influence of system parameters on main body (tank) motion

This section focuses on the main body (tank) motion. In this case, the system parameters, λ, $\bar{\beta}$, and γ were assumed to be constant, while h_0, $\bar{\rho}$, and $\bar{m}_t$ were varied.

4.3.3.1. Influence of liquid height h_0

Figure 6 (a) shows the variations of the main body amplitude y_M with liquid height h_0 for three contact angles: $\theta_0 = 60°$, $90°$, and $100°$ ($\bar{m}_t = 10$). In the figure, the amplitude of the main body motion y_M was included when the maximum sloshing amplitude corresponded to unity. The solid line (blue) and dashed line (red) show the results for the first and second sloshing modes, respectively. It was observed that the former exceeded the latter at $\theta_0 = 60°$, and the motions were opposed, while at $\theta_0 = 100°$, the directions were inter-changed through zero at $\theta_0 = 90°$. It was found that the direction of motion of the main body due to sloshing was dependent on both the sloshing mode number and the contact angle either smaller or greater than $\theta_0 = 90°$. That is, the influence of the sloshing motion on the main body corresponded to zero when $\theta_0 = 90°$.

The maximum main-body amplitude was observed at $0.3 \leq h_0 \leq 0.4$ for the first sloshing mode and at $0.2 \leq h_0 \leq 0.3$ for the second sloshing mode when $\theta_0 = 60°$, and at $0.05 \leq h_0 \leq 0.15$ for the first mode and at $0.15 \leq h_0 \leq 0.25$ for the second mode when $\theta_0 = 100°$. That is, the maximum amplitude of the main modes was observed at low values of h_0. A similar phenomena was observed in experimental and theoretical studies on coupled sloshing motion in a cylindrical tank with an elastic bottom on the earth [19, 20].

4.3.3.2. Influence of tank mass ratio $\bar{m}_t$

Figure 6 (b) shows the variations of the main body amplitude y_M with tank mass ratio $\bar{m}_t$ for three contact angles $\theta_0 = 60°$, $90°$, and $100°$ ($h_0 = 1$). The results indicated that the amplitude of the main body motion increased with decreases in the tank mass ratio $\bar{m}_t$, that is, the main body with a small mass was easily influenced by the sloshing.

4.3.3.3. Influence of density ratio $\bar{\rho}$

The influence of the density ratio $\bar{\rho}$ was investigated in the range $7 \leq \bar{\rho} \leq 50,$ but the influence was not significant, and the results are omitted here.

Generally, as seen in the aforementioned results, the influence of the sloshing motion on the main body was significant when the mass of the main body (tank) was small, and the contained liquid height was also small. The vibration modes of the liquid surface and the amplitude of the main body are illustrated in Fig. 7 when (a) $\theta_0 = 60°,$ and $h_0 = 0.3,$ and (b) $\theta_0 = 100°,$ and $h_0 = 0.15 \, (\bar{\rho} = 1, \ \bar{m}_t = 1).$ In the figures, two arrows indicate the origin of the coordinate in the inertia reference, and the dotted line indicates the difference between the horizontal inertia reference and the liquid height line corresponding to the amplitude of the main body. The red line on the right-hand side corresponds to the beam, although it is rigid in this case. In both cases, the main body displacement was larger in the first sloshing mode, and their directions were opposite to each other as shown in the results in Fig. 6. In comparison with Fig. 4 which shows the results of an anchored tank, the influence of sloshing motions on the main body is clearly shown in Fig. 7.

4.4. Coupled system without liquid

Next a coupled spacecraft system in which the liquid is empty in the tank is considered, which corresponds to a scenario in which the spacecraft runs out of fuel.

The system parameters in this case include beam length ratio $\lambda,$ and tank mass ratio $\bar{m}_t.$ The liquid displacement vector $\mathbf{A}$ was omitted from the frequency equation (36).

Variations of the coupled natural circular frequency Ω with mass ratio $\bar{M}$ ($\bar{M} = \bar{m}_f + \bar{m}_t = \bar{m}_t$ in the case) are shown in Fig. 8. As the mass ratio is defined as $\bar{M} = m_t / 2\rho_b Al,$ the reduction of $\bar{M}$ corresponded to either a decrease in tank mass $\bar{m}_t$ (keeping the length of the beams), or an increase in the length of beams (keeping the tank mass $\bar{m}_t$ constant). In the figure, the natural circular frequencies of a clamp-free beam are depicted with dashed lines. From Fig. 8, with an increase in $\bar{M}$, the natural circular frequency tends to correspond to that of a clamp-free beam ($\Omega_\infty = 3.516, 22.03,$ and 61.69), while a decrease in $\bar{M}$ causes the natural circular frequency to tend to correspond to that of a free-free beam with length $2l$ ($\Omega_0 = 5.593, 30.22,$ and 74.63).

Variations of the corresponding vibration mode on the right-hand side of beam are shown in Fig. 9, with $\bar{M} = 0, 0.5, 1, 5, 10,$ and 100, from which the influence of $\bar{M}$ is evident. When $\bar{M} = 0,$ the point at $\xi = 0$ corresponded to the middle point of the beam with length $2l$, and this point vibrated significantly as a loop of vibration. Increases in $\bar{M}$, decreased the displacement of the main body of the spacecraft fixed at this point, and it tended to zero when $\bar{M} = 100,$ i.e. a point at $\xi = 0$ is a clamped condition, from which it was observed that the amplitude of the main body increased when the tank mass ratio $\bar{M}(m_t)$ and the liquid mass m_f were low.

It should be noted here that when $\bar{M}$ was low, the main body (at $\xi = 0$) moved in a negative direction in the first and the third modes, while it moved in a positive direction in the second mode.

4.5. Coupled system

Finally, a flexible spacecraft with liquid on-board was considered. The system parameters included $\bar{m}_t = 1,$ $\bar{\beta} = 10,$ $\lambda = 10,$ and $h_0 = 1.$

4.5.1. Coupled natural frequency

First, variations of the coupled natural circular frequencies with density ratio $\bar{\rho}$ are shown in Fig. 10(a), in which coupled natural circular frequency curves are represented as solid lines, those when beams are assumed to be rigid using dashed lines, and the coupled natural circular frequency curve when the liquid is empty by dotted lines. From Fig. 10(a), the marked region, which represents the coupled frequency curves crossing area, was magnified in Fig. 10(b).

It was observed that with an increase in $\bar{\rho}$, the coupled natural circular frequency curves decreased along the dashed lines that corresponded to those when the beams were rigid, and the frequency curves of this type corresponded to those in which liquid sloshing was predominant. Additionally, in another type of vibration curve parallel to dotted line, the beam vibration was predominant. At some points, these two vibration curves crossed each other.

The natural circular frequency curves for the case where $\theta_0 = 90°$ exhibited a similar tendency.

4.5.2. Coupled vibration mode and CEV

Figure 10(b) shows the variation of vibration modes at the region where the two frequency curves crossed. The term coupling evaluation value (CEV) [17] was introduced to observe the coupling strength between beam motion and liquid motion as follows:

$$CEV = |w(1)| \times |\zeta/\lambda|, \tag{38}$$

which was composed of displacements at the free end of the beam and the maximum displacement of the liquid. Additionally, an increase in the above value increased the strength of the coupling between the beam motion and the liquid motion. In Eq. (38), ζ was divided by λ to compare two displacements, since the non-dimensional displacement of beam w was normalized by l while the non-dimensional displacement of the free surface was normalized by R.

Variations of vibration mode and CEV are shown in Fig. 11. In this region, coupling existed between the second mode and the third mode; the CEV is represented in the upper diagram.

The first mode involved the first sloshing mode that was independent of the $\bar{\rho}$ value, and neither beam motion nor main body motion was observed. In contrast, in the second mode and the third mode, all the beams, the free surface, and the main body were observed to have motion. In the second mode, the beam motion was predominant at $\bar{\rho} \leq 1.95$, and the free surface motion was predominant at $2.1 \leq \bar{\rho}$. While in the third mode, the free surface motion was predominant at $\bar{\rho} \leq 1.95$, and the beam motion was predominant in the $2.1 \leq \bar{\rho}$ region, which suggested that the exchange of the predominant mode occurred at $\bar{\rho} \approx 2.0$.

With respect to the CEV, the CEV of the second mode was higher, up to $\bar{\rho} = 1.95$, and that of the third mode was higher in the region greater than $\bar{\rho} = 2.1$. Additionally, the CEV was high in the vicinity of the crossing point at $\bar{\rho} \approx 2.0$. In the actual satellite motion, given these system parameters, the main body motion was significant when the beam motion was predominant.

Similar diagrams for $\theta_0 = 90°$ are shown in Fig. 12. This is contrary to the results for $\theta_0 = 60°$ shown in Figure 11, as no motion was observed on the free surface in the second mode in which beam motion was predominant. Furthermore, the exchange of vibration modes appeared in a very narrow region,

17

$2.4 < \bar{\rho} < 2.45$, and therefore CEV corresponded to zero along the whole $\bar{\rho}$ value, which indicated that there was no coupling except for a very narrow region when $\theta_0 = 90°$.

It should be noted that the tendency for the $\theta_0 = 100°$ case was similar to that for $\theta_0 = 60°$ case (the results are omitted here).

4.5.3. Influence of liquid height

In an actual spacecraft, the volume of liquid on-board will decrease during the mission (i.e. with time). The influence of the liquid height h_0 on the coupled natural frequency and vibration mode are investigated in this section.

Figures 13(a) and 13(b) represent the variations of the coupled natural circular frequency with liquid height h_0 for the $\theta_0 = 60°$ and $90°$ cases, respectively ($\bar{\rho}=1$, $\gamma=1\times10^{-4}$, $\lambda=10$, $\bar{\beta}=10$, and $\bar{m}_t=1$). In each figure, variations of the coupled natural frequency curves up to the fifth mode are shown on the left-hand side as (i). Additionally, the magnified view around the crossing region of the second sloshing mode (pink) and the first beam mode curves are shown on the right-hand side as (ii). In both figures, given that the two frequency curves crossed near $h_0 = 0.17$ for $\theta_0 = 60°$, and near $h_0 = 0.08$ for $\theta_0 = 90°$, with decreases in the liquid height coupling between the liquids, the main body (tank) and the beams motions were expected to be significant. The crossing region for $\theta_0 = 60°$ in Fig. 13(a)(ii) is wider than that for $\theta_0 = 90°$ in Fig. 13(b)(ii).

Vibration modes for three liquid heights in the $\theta_0 = 60°$ case in Fig. 13(a) are shown in Fig. 14(a). At $h_0 = 0.17$, the liquid motion and the beam motion indicated strong coupling, and the main body motion was significant when the beam motion was high, and the exchange of vibration modes occurred at this liquid height.

Similar results are shown in Fig. 14(b) when $\theta_0 = 90°$, in which the exchange of vibration modes occurred at $h_0 = 0.08$. This differs from Fig. 14(a) when $\theta_0 = 60°$, and coupling between the liquid motion and the beam motion was zero as shown in Fig. 12 when $\theta_0 = 90°$.

5. Conclusions

This study involved the analysis of the influence of liquid sloshing on the dynamics of flexible space structures with on-board liquid in zero-gravity conditions. The main body of the spacecraft was modelled as a rigid tank, the flexible appendages as two elastic beams, and the on-board liquid as an ideal liquid. The obtained results are summarized as follows:

ⅰ) *Sloshing characteristics in an anchored tank without beam*

- Maximum natural sloshing frequency was observed at a contact angle $\theta_0 = 90°$, while the natural frequency decreased with decreases or increases in θ_0 from $\theta_0 = 90°$.

- With an increase in the liquid height h_0, the natural frequency increased and reached a saturation value. Both the above results corresponded to those obtained by Bauer et al [2].

- The sloshing vibration mode showed slight variations with respect to contact angle θ_0.

ⅱ) *Sloshing characteristics in a tank floating in space*

The results that varied from those in the case of the anchored tank mentioned above included the following:

- Natural sloshing frequencies were slightly higher than those in the anchored tank.

- The sloshing motion of the liquid influenced the freely floating main body and caused its motion. The direction of the main body was opposite in the $\theta_0 < 90°$, and $90° < \theta_0$ cases and was different from the vibration mode of sloshing. However, at $\theta_0 = 90°$, liquid sloshing did not influence the motion of the main body.

- The influence of the sloshing motion on the main body motion increased with decreases in the tank mass ratio $\bar{m}_t$ and liquid height h_0.

ⅲ) *Coupled system without liquid*

- When the tank mass ratio $\bar{m}_t$ was high, the main body did not show any motion, and the natural frequency tended to correspond to that of a clamp-free beam.

- When the tank mass ratio $\bar{m}_t$ was low, the natural frequency tended to correspond to that of a free-free beam with length $2l$, in which the vibration mode (as the main body was located at the middle of the free-free beam) took the root of vibration, and the amplitude increased. The direction of motion of the main body was in the negative direction for the odd-order vibration mode, and in the positive direction for the even-order vibration mode, given that the amplitude of the free end of the beams was in the positive direction. These corresponded to the same results as those obtained in a mechanical model in a previous study [17].

ⅳ) *Coupled system*

- In a mechanical model [17] in which the on-board liquid was modelled as a "spring-mass" system, there was only one natural sloshing frequency. However, in the present model in which the on-board liquid was modelled as an ideal fluid, infinite numbers of natural sloshing frequencies existed. Therefore, an

infinite number of coupling regions existed between the liquid motion and beam motion.

- For example, in the diagram illustrating variations of the coupled natural frequency with density ratio $\bar{\rho}$, two natural frequency curves, namely one in which the liquid motion was predominant and the other in which the beam motion was predominant, intersected each other. In the crossing region at which $\theta_0 = 90°$, the coupling region in which the liquid motion and beam motion coupled was very narrow. In contrast, when the contact angle corresponded to $\theta_0 \neq 90°$, (for example, $\theta_0 = 60°$, and $100°$,) the two motions coupled with each other in a wide region.

- During the operation of satellites, decreases in fuel may lead to the crossing of two natural frequencies that would introduce strong coupling of the two motions, i.e. liquid sloshing and beam vibration.

- In the coupled vibration mode in which the beam motion was predominant, the main body motion became significant at a lower tank mass ratio $\bar{m}_t$. The direction of motion of the main body depended on the order of vibration of the beam: i.e. in the odd-order mode, the direction was opposite relative to the beam tip motion, and in the even-order mode, the direction corresponded with that of the beam tip motion.

- With respect to the free surface motion during coupling, the free surface did not move when $\theta_0 = 90°$ even if the main body (tank) moved, while at $\theta_0 \neq 90°$, a vibration appeared on the free surface, i.e. sloshing occurred.

Appendix A. Eigenfunctions of the beam [17]

The eigenfunctions of the beam that satisfy the boundary conditions in Eq. (12)", i.e. mass-free:

$$\tilde{w}_{im}\left(\xi_i\right) = \cosh\alpha_m\xi + \frac{1}{2}\bar{M}\alpha_m\left(\sinh\alpha_m\xi_i - \sin\alpha_m\xi_i\right)$$

$$-\frac{\sinh\alpha_m + \frac{1}{2}\bar{M}\alpha_m\left(\cos\alpha_m + \cosh\alpha_m\right)}{\sin\alpha_m + \frac{1}{2}\bar{M}\alpha_m\left(\cos\alpha_m + \cosh\alpha_m\right)}\left(\cos\alpha_m\xi_i + \frac{1}{2}\bar{M}\alpha_m\left(\sinh\alpha_m\xi_i - \sin\alpha_m\xi_i\right)\right) \quad \text{(A1)}$$

where α_m denotes the parameters that satisfy the following frequency equation:

$$\sinh\alpha_m\cos\alpha_m + \cosh\alpha_m\sin\alpha_m + \bar{M}\alpha_m\left(1 + \cos\alpha_m\cosh\alpha_m\right) = 0 \quad \text{(A2)}$$

Eigenfunction $\tilde{w}_{im}\left(\xi_i\right)$ has the following characteristics in its integration:

$$X_{mn}^{00} = \int_0^1 \tilde{w}_{im}\left(\xi_i\right)\tilde{w}_{in}\left(\xi_i\right)\mathrm{d}\xi_i = \begin{cases} -\bar{M}\tilde{w}_{in}\left(0\right)\tilde{w}_{im}\left(0\right) & :m \neq n \\ \frac{1}{4}\left(\tilde{w}_{in}^2\left(1\right) - 3\bar{M}\tilde{w}_{in}^2\left(0\right)\right) & :m = n \end{cases}$$

$$\quad \text{(A3)}$$

$$X_{mn}^{22} = \int_0^1 \frac{\mathrm{d}^2\tilde{w}_{im}\left(\xi_i\right)}{\mathrm{d}\xi_i^2}\frac{\mathrm{d}^2\tilde{w}_{in}\left(\xi_i\right)}{\mathrm{d}\xi_i^2}\mathrm{d}\xi_i = \begin{cases} 0 & :m \neq n \\ \frac{1}{4}\alpha_n^4\left(\tilde{w}_{in}^2\left(1\right) + \bar{M}\tilde{w}_{in}^2\left(0\right)\right) & :m = n \end{cases}$$

Appendix B. System parameters range

Table B1 shows the specifications of a few Japanese satellites and the corresponding estimated values for $\bar{M}$, λ, and $\bar{\beta}$. In the table, radius R of the cylinder in the model was obtained as half of the satellite's length in the crosswise direction, and the mass of paddles and ratio of the mass were estimated assuming that the power generation of the solar array paddle was in the range of $20-100$ W/kg. The tank mass was estimated assuming that 20% of the launch mass of the satellite corresponded to liquid fuel, and the tank mass ratio $\bar{m}_t$ was obtained by subtracting the fuel mass and the paddle mass from the launch mass. The thickness of the solar array paddle was assumed as 12.5 mm for all the satellites. Three types of liquid, i.e., hydrazine, nitrogen peroxide, and water, are considered in Table B2.

- Tank mass ratio $\bar{m}_t$: From Table B1, $\bar{m}_t = 4.97-137$, and subsequently $\bar{m}_t = 1-100$.
- Density ratio $\bar{\rho}$: From Table B2, $\bar{\rho} = 7.6-48.1$, and subsequently $\bar{\rho} = 7-50$.
- Area ratio of beam and tank $\bar{\beta}$: From Table B1, $\bar{\beta} = 8.58-101.0$, and subsequently $\bar{\beta} = 10-100$.
- Ratio of the length of elastic beam and the tank radius λ: From Table B1, $\lambda = 2.46-13.9$, and subsequently $\lambda = 1-10$.
- Bending rigidity of beam: It was assumed that the beam was sandwiched between two face skins with an aluminium honeycomb core (see Fig. B1). The bending rigidity of the core was ignored, and it was assumed that the two skins had the same thickness and were of the same material to obtain the bending rigidity of the sandwich beam EI from Eq. (B1) as follows:

$$EI = b\left\{\frac{E_f t_f h^2}{2} + \frac{E_f t_f^3}{6}\right\}$$

(B1)

where

$$h = t_c + \frac{t_{f1} + t_{f2}}{2}$$

(B2)

where t_c denotes core thickness and t_f denotes skin thickness. Furthermore, when the skins are thin, the following expression is obtained:

$$EI = \frac{E_f t_f b h^2}{2}$$

(B3)

Here, the skin was assumed to be made of CFRP(Carbon Fibre Reinforced Plastics) with Young's modulus $E_f = 55-560$ GPa and thickness $t_f = 0.1$ mm. The estimated bending rigidity and the surface tension parameter γ are shown in Table B3. From Table B3, $\gamma = (0.287-35.4)\times 10^{-6}$ and subsequently $\gamma = 10^{-7} - 10^{-4}$. The range of system parameters is summarized in Table B4.

References

[1] H.N. Abramson, *The dynamic behaviour of liquids in moving containers*, chapter 11, NASA SP-106. (1966)

[2] H.F. Bauer, W. Eidel, Linear liquid oscillations in cylindrical container under zero gravity, *Appl. Microgravity tech, II* (1990) 212-220.

[3] H.F. Bauer, W. Eidel, Small amplitude liquid oscillations in a rectangular container under zero gravity, *Zeitsschrift fur Flugwissenschaften und Weltraumforschung* **14** (1990) 1-8.

[4] B.N. Agrawal, Dynamic characteristics of liquid motion in partially filled tanks of a spinning spacecraft, *J. Guidance, Control, and Dynamics* **16**(4) (1993) 636-640.

[5] K. Komatsu, Modeling of the dynamic behaviour of liquids in spacecraft, *Int. Journal of Microgravity Science and Application* **16**(3) (1999) 182-190.

[6] M. Chiba, H. Watanabe, H.F. Bauer, Hydroelastic coupled vibrations in a cylindrical container with a membrane bottom, containing liquid with surface tension, *Journal of Sound & Vibration* **251**(4) (2002) 717-740.

[7] M. Utsumi, A mechanical model for low-gravity sloshing in an axisymmetric tank, *Trans. ASME, Journal of Applied Mechanics* **71** (2004) 724-730.

[8] H. Yuanjun, M. Xingrui, W. Pigping, W. Benli, Low-gravity liquid nonlinear sloshing analysis in a tank under pitching excitation, *Journal of Sound and Vibration* **299** (2007) 164-177.

[9] M.D. Berglund, C.E. Bassett, J.M. Kelso, J. Mishic, D. Schrange, The Boeing Delta IV launch vehicle–Pulse-settling approach for second-stage hydrogen propellant management, *Acta Astronautica* **61** (2007) 416-424.

[10] J.P.B. Vreeburg, Sloshsat spacecraft calibration at stationary spin rates, *Journal of Spacecraft and Rockets* **45**(1) (2008) 65-75.

[11] J.E. McIntyre, J.M. McIntyre, Some effects of propellant motion on the performance of spinning satellites, *Acta Astronautica* **9**(12) (1982) 645-661.

[12] P. Santini, R. Barboni, Motion of orbiting spacecrafts with a sloshing fluid, *Acta Astronautica* **5**(7-8) (1978) 467-490.

[13] P. Santini, R. Barboni, A minicomputer finite elements program for microgravity hydroelastic analysis, *Acta Astronautica* **10**(2) (1983) 81-90.

[14] L. Jing, L. Jun-feng, W. Tian-shu, Dynamic response of liquid filled rectangular tank with elastic appendages under pitching excitation, *Applied Mathematics and Mechanics* **28**(3) (2005) 351-359.

[15] V.A. Buzhinskii, The equations of the perturbed motion of a rocket as a thin-walled structure with a liquid, *Journal of Applied Mechanics* **73** (2009) 692-695.

[16] C. Farhat, E.K. Chiu, D. Amsallem, Modeling of fuel sloshing and its physical effects on flutter, *AIAA Journal* **51**(9) (2013) 2252-2265.

[17] M. Chiba, S. Chiba, K. Takemura, Coupled hydroelastic vibrations of a liquid on flexible space structures under zero-gravity– part I. mechanical model, *Coupled Systems Mechanics* **2**(4) (2013) 303-327.

[18] J. C. Luke, A variational principle for a fluid with a free surface, *Journal of Fluid Mechanics* **27**(2) (1967) 395-397.

[19] M. Chiba, Nonlinear hydroelastic vibration of a cylindrical tank with an elastic bottom, containing liquid, part Ⅰ: experiment, *Journal of Fluids & Structures* **6**(2) (1992) 181-206.

[20] M. Chiba, The influence of elastic bottom plate motion on the resonant of a liquid free surface in a cylindrical container: a linear analysis, *Journal of Sound & Vibration* **202**(3) (1997) 417-426.

Tab. 1 Nomenclature : (non-dimensional)

A	Cross sectional area of beam	$z_0(r)$	Static liquid free surface : $\left(\eta_0 = z_0 / R\right)$
b	Length of tank	$Z(r,\varphi,t)$	Amplitude of liquid surface
E	Young's modulus of beam		: $\left(\zeta = Z / R\right)$
h	Equivalent liquid height	$Z_f(r,\varphi,t)$	Displacement of liquid free surface
	: $\left(h_0 = h / R\right)$	$\Phi(r,\varphi,z,t)$	Liquid velocity potential
I	Second moment of area of beam		: $\left(\phi = \Phi / \omega_b R^2\right)$
l	Length of beam $\left(\lambda = l/R\right)$	θ_0	Static contact angle of liquid
m_f	Mass of liquid : $\left(\bar{m}_f = m_f / 2\rho_b Al\right)$	ρ_f	Density of liquid
m_t	Mass of rigid tank	ρ_b	Density of beam
	: $\left(\bar{m}_t = m_t / 2\rho_b Al\right)$	σ	Coefficient of free surface tension
M	Summation of m_f and m_t		: $\left(\gamma = \sigma R^2 l / EI\right)$
	: $\left(\bar{M} = \bar{m}_f + \bar{m}_t\right)$	$\bar{\beta}$	Area ratio of beam and tank $\left(= \pi R^2 / 2A\right)$
o$-XY$	Coordinate system for spacecraft	$\bar{\rho}$	Density ratio $\left(= \rho_f / \rho_b\right)$
o$-r\varphi z$	Coordinate system for tank	ω_b	Natural circular frequency of beam
	: $\left(\text{o}-\rho\varphi\eta\right)$		$\left(= \sqrt{EI / \rho_b Al^4}\right)$
R	Radius of rigid tank	ξ_i	Non-dimensional coordinate : $\left(= x_i / l\right)$
t	Time : $\left(\tau = \omega_b t\right)$	ω	Coupled natural circular frequency
Y_M	Displacement of rigid tank		$\left(\Omega = \omega / \omega_b\right)$
	: $\left(y_M = Y_M / l\right)$		
$W_i(x_i, t)$	Displacements of beams		
	: $\left(w_i = W_i / l\right)$		

Table A1 Specifications of satellite and parameters

Satellite		Launch mass [kg]	Dimensions [m]	Power [W]	Dimension of paddle [m]	Mass of paddle [kg]	$\bar{m}_t$ $(= m_t/2\rho_b Al)$	λ $(= l/R)$	$\bar{\beta}$ $(= \pi R^2/2A)$
ETS-VIII	Large	2800	$2.35 \times 2.45 \times 7.3$	7500	約 17×2	$75 \sim 375$	$4.97 \sim 28.9$	13.9	57.5
DRTS	Large	2800	$2.2 \times 2.4 \times 2.2$	2100	7.3×2.4	$21 \sim 105$	$20.3 \sim 106$	6.10	44.0
TRMM	Large	3620	$3.0 \times 3.5 \times 5.1$	3300	4.3×2.1	$33 \sim 165$	$16.6 \sim 86.8$	2.46	101.0
EOS-PM	Large	3100		4860		$49 \sim 243$	$9.21 \sim 50$		
ALOS	Large	4000	$3.5 \times 4.0 \times 6.2$	7000	8.9×3.1	$70 \sim 350$	$8.14 \sim 44.7$	4.45	90.9
GOSAT	Large	1650	$2.4 \times 2.6 \times 2.7$	3300	約 6×3	$33 \sim 165$	$7 \sim 39$	4.62	41.6
WINDS	Large	2700	$2.0 \times 3.0 \times 8.0$	5200	約 6×3	$52 \sim 260$	$7.31 \sim 40.5$	4.00	40.0
OICETS	Middle	570	$0.78 \times 1.1 \times 1.5$	1220	約 4×2	$12.2 \sim 61$	$6.48 \sim 36.4$	7.27	8.58
SWAS	Small	102		59		$1 \sim 3$	$26.7 \sim 137$		

Table A2 Specifications of liquid

| Material	Density ρ_f or ρ_b [kg/m³]	Coefficient of surface tension σ [mN/m]	Density ratio $\bar{\rho}(=\rho_f/\rho_b)$
Hydrazine	1004	66.5	7.7～33.5
Nitrogen peroxide	1443	25.1	11.1～48.1
Water	1000	71.7	7.6～30
Al honeycomb	30～130	—	

Table A3 Bending stiffness of honeycomb beam and corresponding surface tension parameters: $\gamma(=\sigma Al/EI)$ ($h=12.5$mm, $t_f=0.1$mm)

Satellite	Bending stiffness $EI\times10^3$ [Nm²]	$\gamma\times10^{-6}$		
		Hydrazine	Nitrogen peroxide	Water
ETS-VIII	0.873~8.89	3.23~32.9	1.22~12.4	3.48~35
DRTS	1.05~10.6	1.39~14.1	0.523~5.33	1.49~15
TRMM	0.917~9.34	0.817~8.32	0.308~3.14	0.881~8
ALOS	1.35~13.8	1.69~17.2	0.638~6.50	1.83~18
GOSAT	1.31~13.3	1.14~11.6	0.430~4.38	1.23~12
WINDS	1.31~13.3	1.14~11.6	0.430~4.38	1.23~12
OICETS	0.873~8.89	0.760~7.74	0.287~2.92	0.819~8

Table A4 Range of parameters

Parameter		Range
$\bar{m}_t$	$m_t/2\rho_b Al$	$1\sim100$
h_0	h/R	$0\sim1$
$\bar{\rho}$	ρ_f/ρ_b	$7\sim50$
γ	$\sigma Al/EI$	$10^{-8}\sim10^{-5}$
$\bar{\beta}$	$\pi R^2/2A$	$10\sim100$
λ	l/R	$1\sim10$
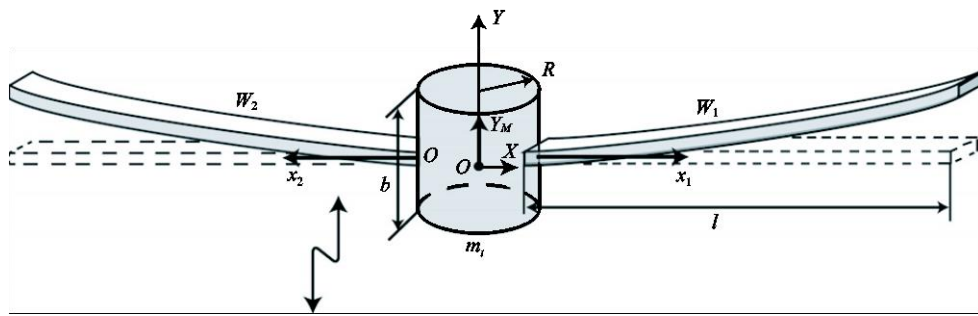
(a)   Spacecraft with two appendages.
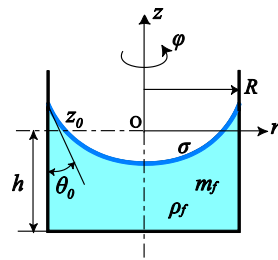
(b)   Cylindrical tank.

Fig. 1 Flexible spacecraft model with liquid tank.; (a) Spacecraft with two appendages.; (b) Cylindrical tank.
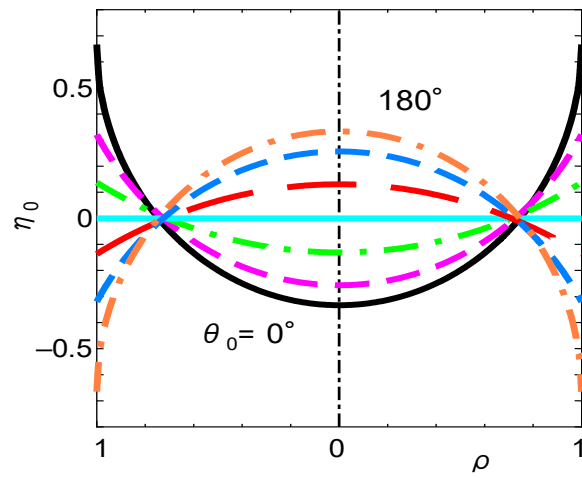
Fig. 2 Meniscus in a cylindrical tank with contact angle θ_0.

(a) $h_0 = 1, \gamma = 1 \times 10^{-6}, \bar{\rho} = 1$ *unregistered*

(b) $\theta_0 = 90^0, \gamma = 1 \times 10^{-6}, \bar{\rho} = 1$ *unregistered*

(c) $h_0 = 1, \theta_0 = 90^0, \bar{\rho} = 1$
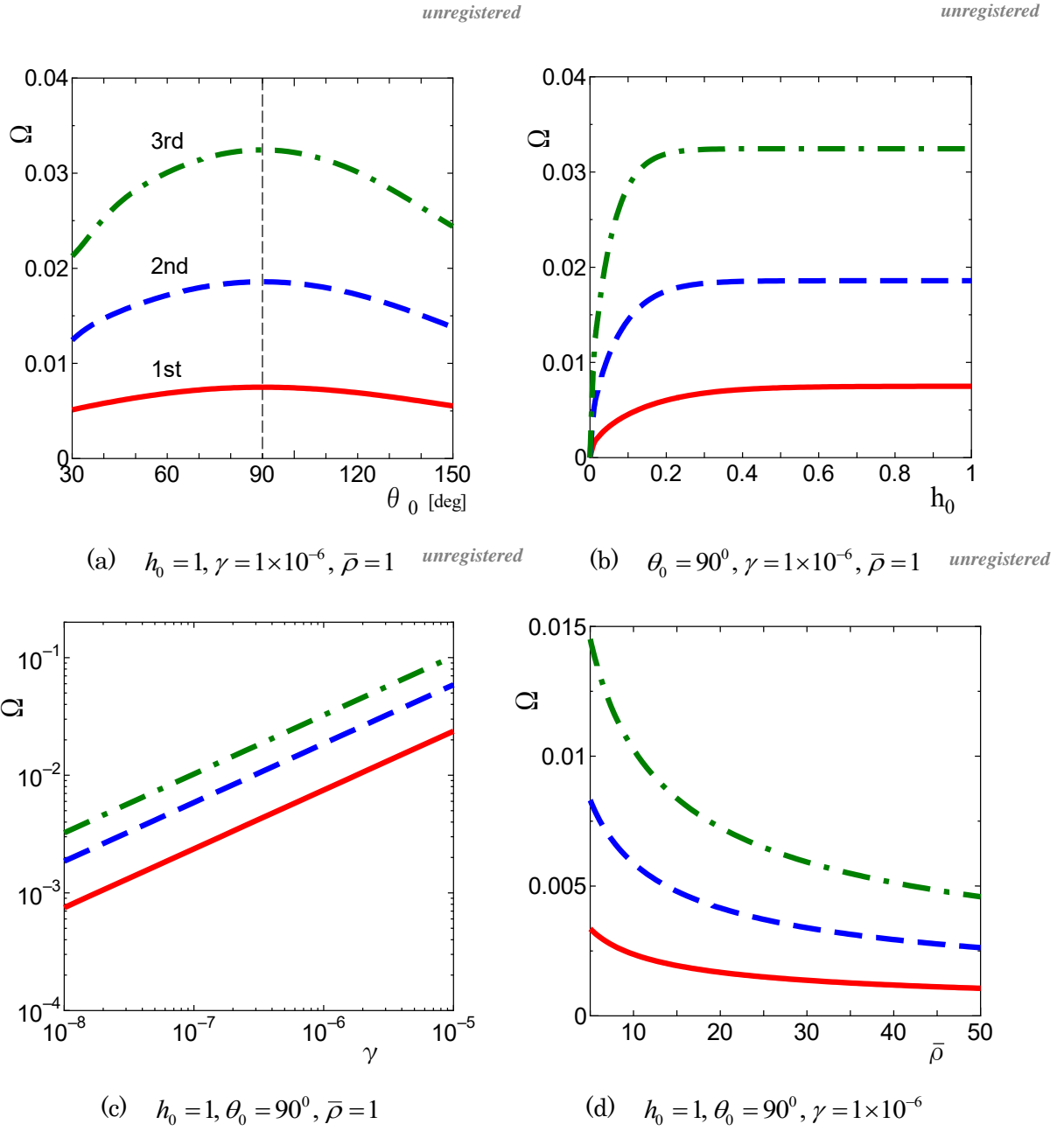
(d) $h_0 = 1, \theta_0 = 90^0, \gamma = 1 \times 10^{-6}$

Fig. 3 Natural sloshing frequencies in an anchored cylindrical tank (without beam : $\lambda = 1$).;

(a) $h_0 = 1, \gamma = 1 \times 10^{-6}, \bar{\rho} = 1$; (b) $\theta_0 = 90^0, \gamma = 1 \times 10^{-6}, \bar{\rho} = 1$; (c) $h_0 = 1, \theta_0 = 90^0, \bar{\rho} = 1$; (d) $h_0 = 1, \theta_0 = 90^0, \gamma = 1 \times 10^{-6}$

3
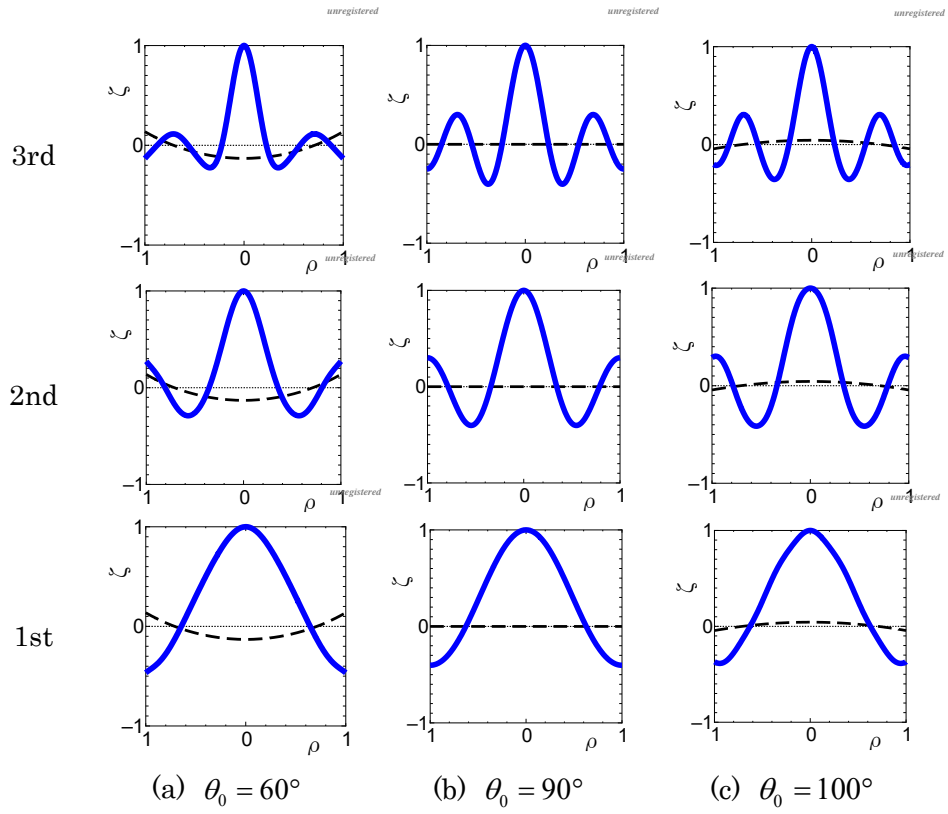
Fig. 4 Variations of sloshing mode with contact angle θ_0 ($h_0 = 1$, $\gamma = 1 \times 10^{-6}$, $\bar{\rho} = 1$, $\lambda = 1$).;

(a) $\theta_0 = 60°$; (b) $\theta_0 = 90°$; (c) $\theta_0 = 100°$
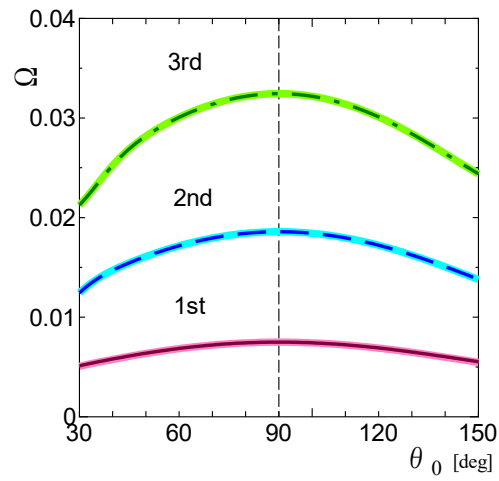
Fig. 5 Variations of natural circular frequency with contact angle θ_0 （floating tank）:

$$\lambda = 1,\ h_0 = 1,\ \gamma = 1 \times 10^{-6},\ \bar{\rho} = 1,\ \bar{m}_t = 10\,.$$

$\theta_0 = 60°$

$\theta_0 = 90°$

$\theta_0 = 100°$
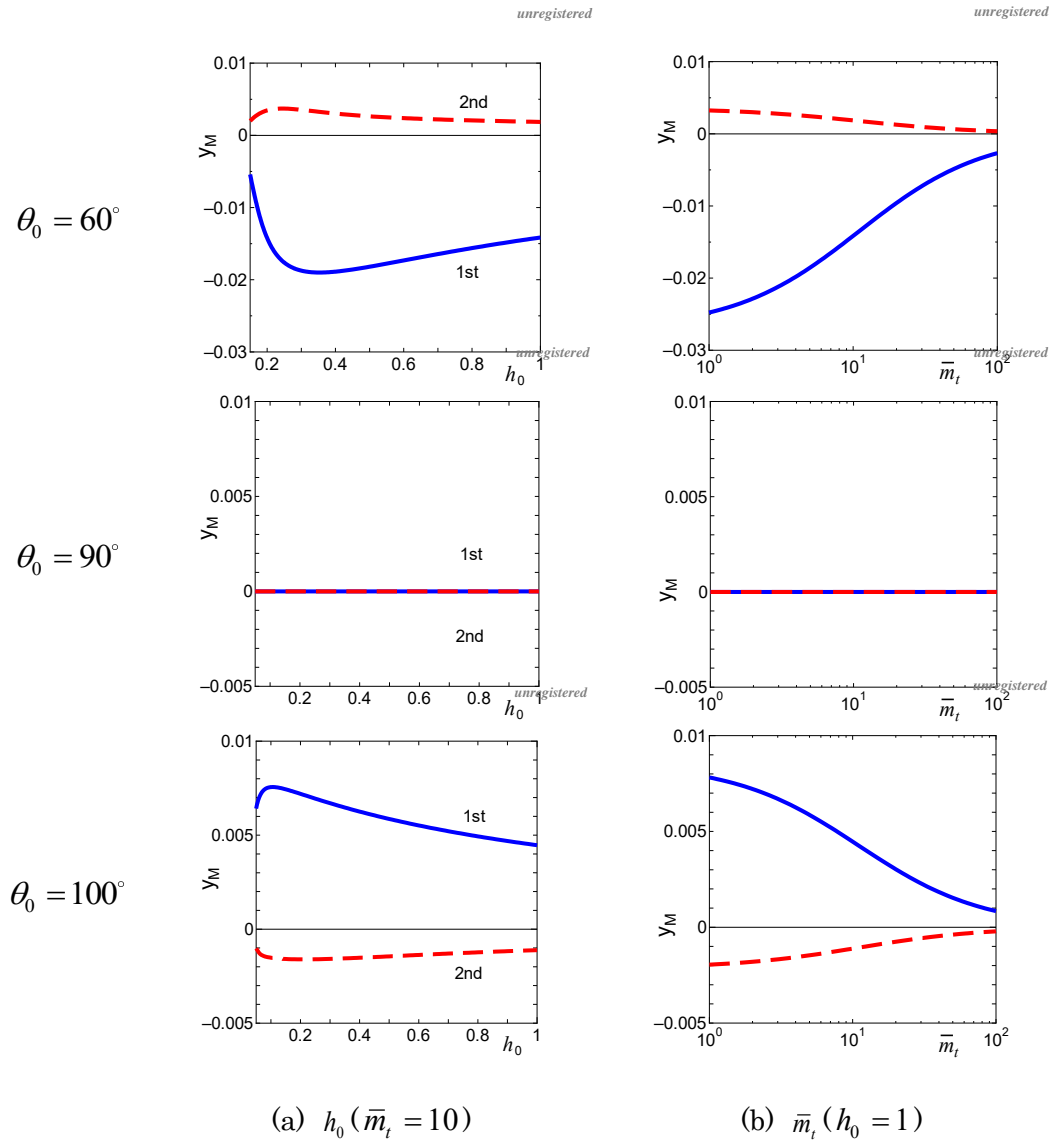
(a) $h_0 \, (\bar{m}_t = 10)$

(b) $\bar{m}_t \, (h_0 = 1)$

Fig. 6 Influences of liquid height h_0 : (a) and mass ratio $\bar{m}_t$: (b) on main body (tank) motion

$(\gamma = 1 \times 10^{-6}, \bar{\rho} = 1, \lambda = 1, \bar{\beta} = 10)$.; (a) $h_0 \, (\bar{m}_t = 10)$; (b) $\bar{m}_t \, (h_0 = 1)$

2nd

1st

(a) $\theta_0 = 60°\,(h_0 = 0.3\,)$ (b) $\theta_0 = 100°\,(h_0 = 0.15\,)$
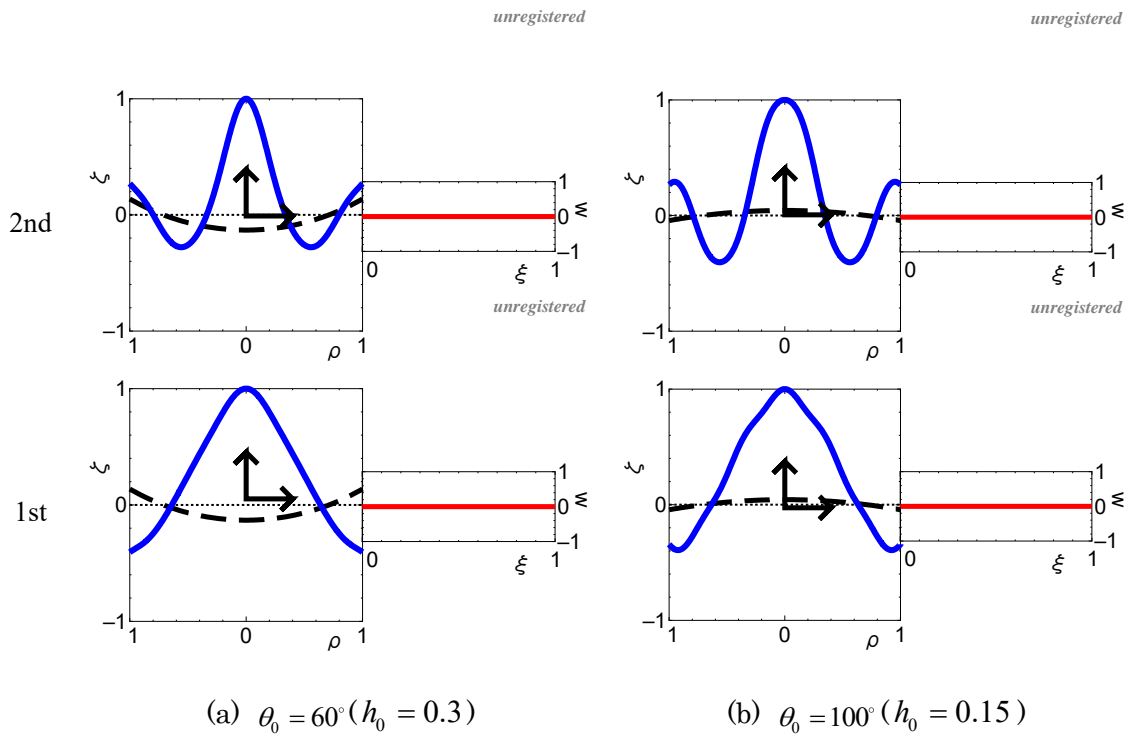
Fig. 7   Liquid sloshing mode and displacement of spacecraft main body (neglecting flexibility of beams)

$(\gamma = 1 \times 10^{-6},\ \bar{\rho} = 1, \bar{m}_t = 1,\ \lambda = 1,\ \bar{\beta} = 10\,)$.; (a) $\theta_0 = 60°\,(h_0 = 0.3\,)$; (b) $\theta_0 = 100°\,(h_0 = 0.15\,)$
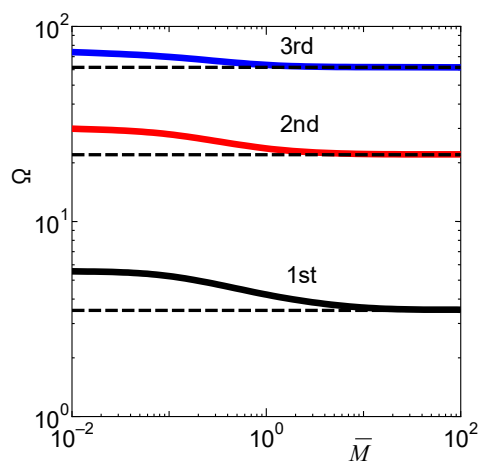
Fig. 8   Influence of mass ratio $\bar{M}$ on natural circular frequency of rigid tank with flexible beam
(without liquid) :   --- : clamp - free beam.

(a) 1st mode   (b) 2nd mode   (c) 3rd mode
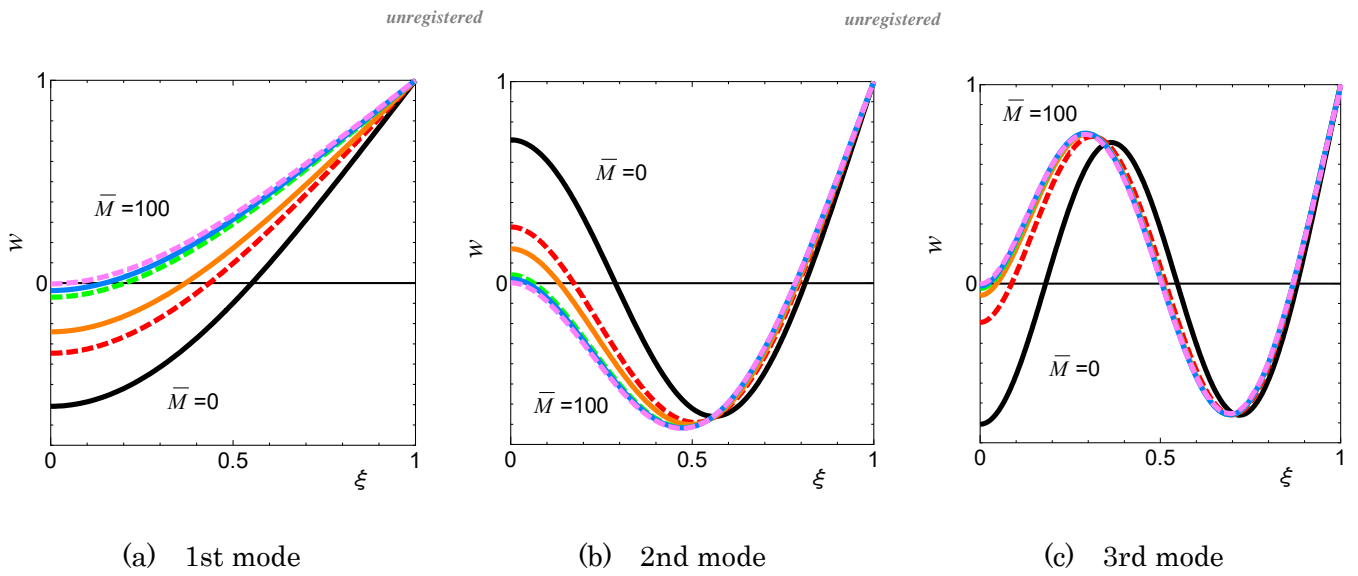
Fig. 9   Vibration mode of beam with rigid mass $\bar{M}$ at its center : Influence of $\bar{M}$

$(\bar{M} = 0, 0.5, 1, 5, 10, 100)$.; (a) 1st mode; (b) 2nd mode; (c) 3rd mode
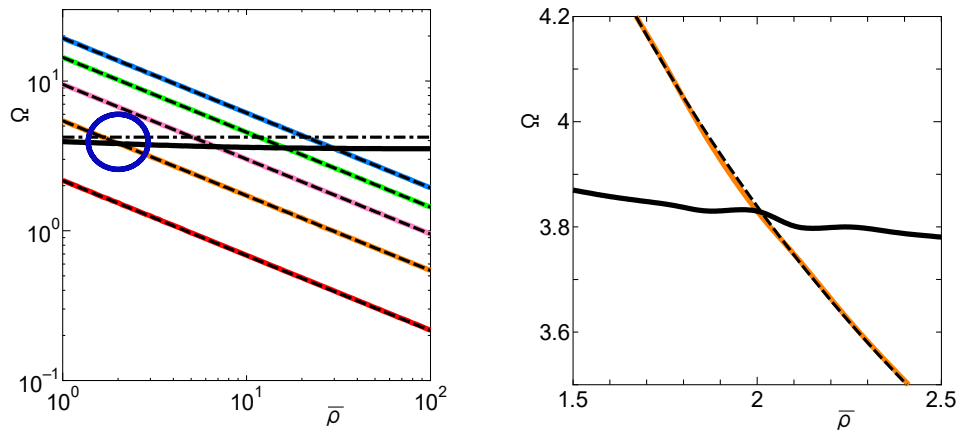
(a)   Natural circular frequency curves.   (b)   Magnified view.

Fig. 10   Variation of coupled natural frequency with density ratio $\bar{\rho}$ ($\theta_0 = 60°, h_0 = 1, \gamma = 1 \times 10^{-4}$, $\lambda = 10, \bar{\beta} = 10, \bar{m}_t = 1$).; (a) Natural circular frequency curves.; (b) Magnified view.
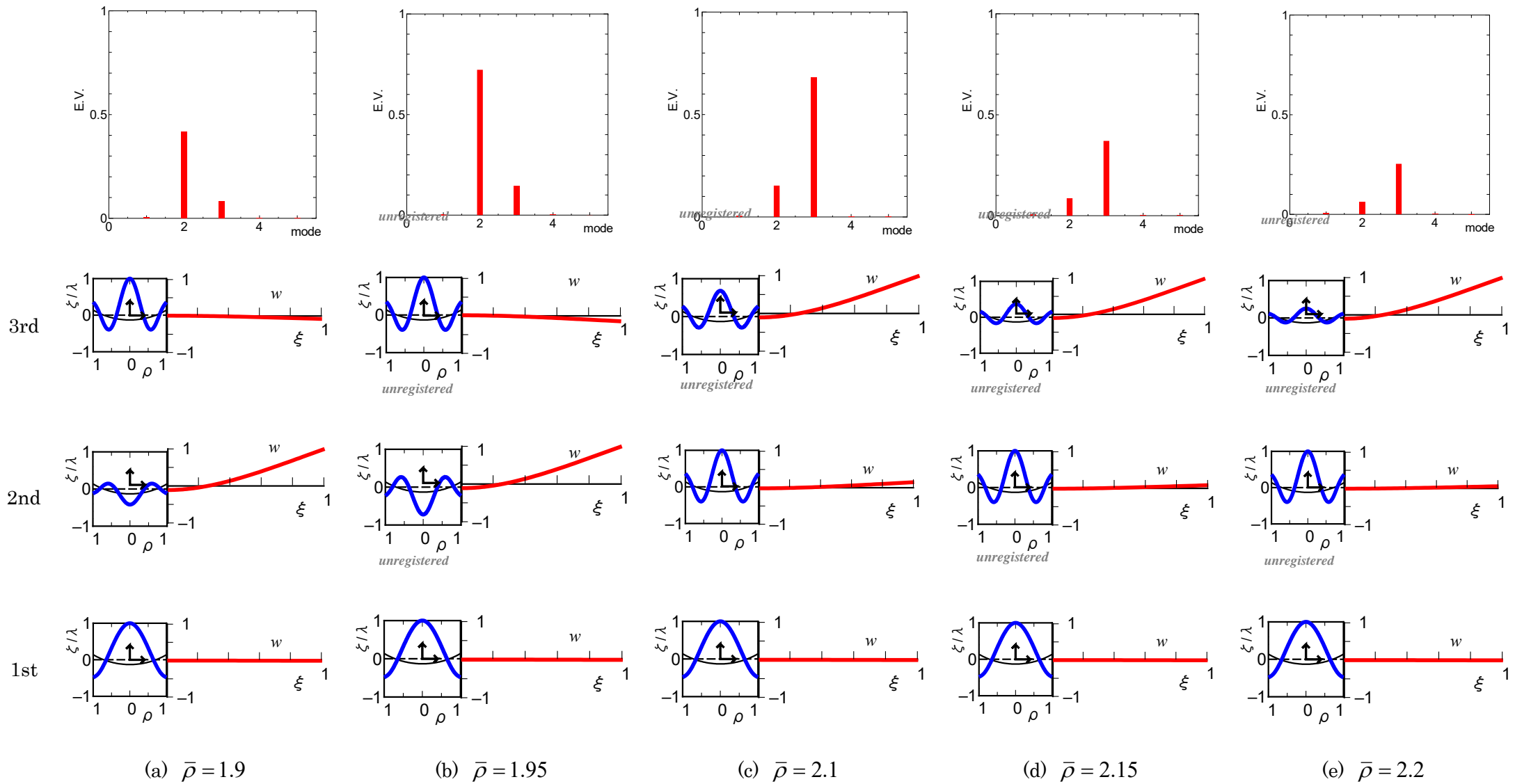
Fig. 11　Variation of coupled vibration mode and *coupling evaluate value CEV* with $\bar{\rho}$ $(\theta_0 = 60°,\ h_0 = 1,\ \gamma = 1\times10^{-4},\ \bar{\beta} = 10,\ \lambda = 10,\ \bar{m}_t = 1)$.;

(a) $\bar{\rho} = 1.9$; (b) $\bar{\rho} = 1.95$; (c) $\bar{\rho} = 2.1$; (d) $\bar{\rho} = 2.15$; (e) $\bar{\rho} = 2.2$

11
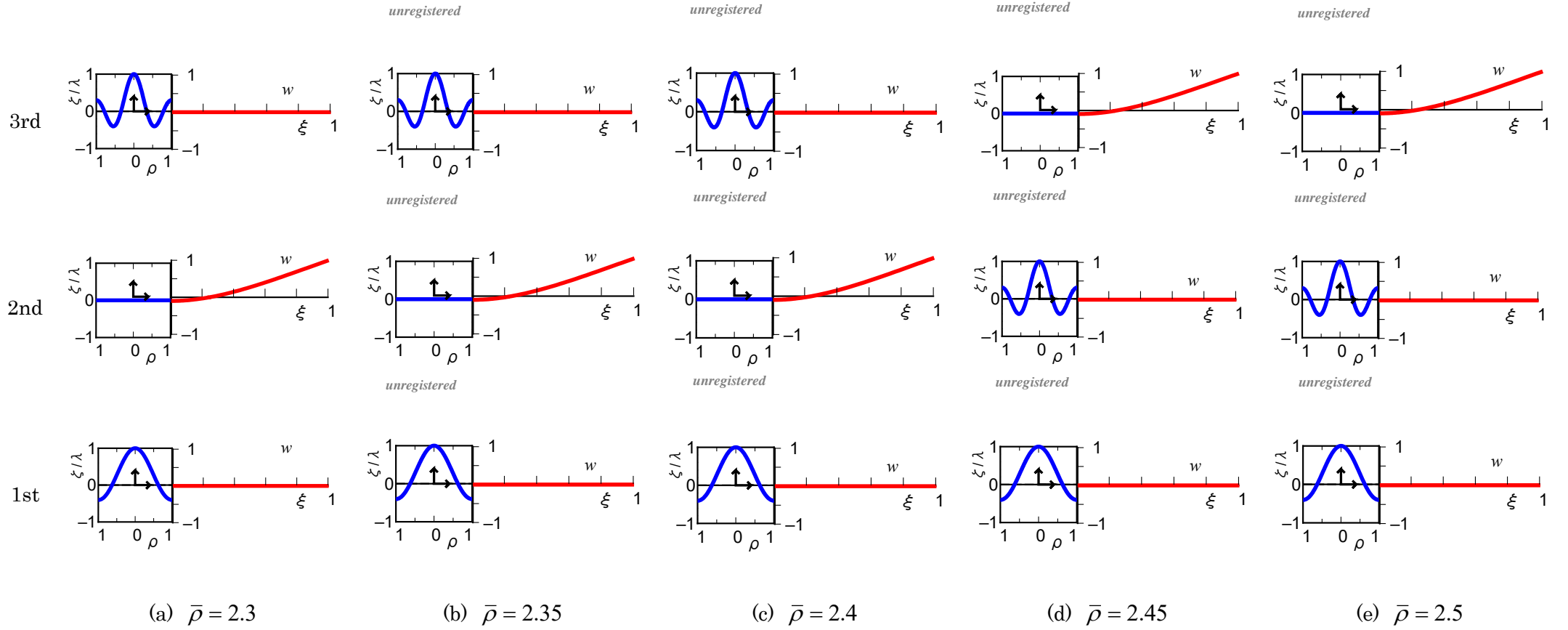
Fig. 12 Variation of coupled vibration mode with $\bar{\rho}$ $(\theta_0 = 90°, h_0 = 1, \gamma = 1 \times 10^{-4}, \bar{\beta} = 10, \lambda = 10, \bar{m}_t = 1)$.;

(a) $\bar{\rho} = 2.3$; (b) $\bar{\rho} = 2.35$; (c) $\bar{\rho} = 2.4$; (d) $\bar{\rho} = 2.45$; (e) $\bar{\rho} = 2.5$

12
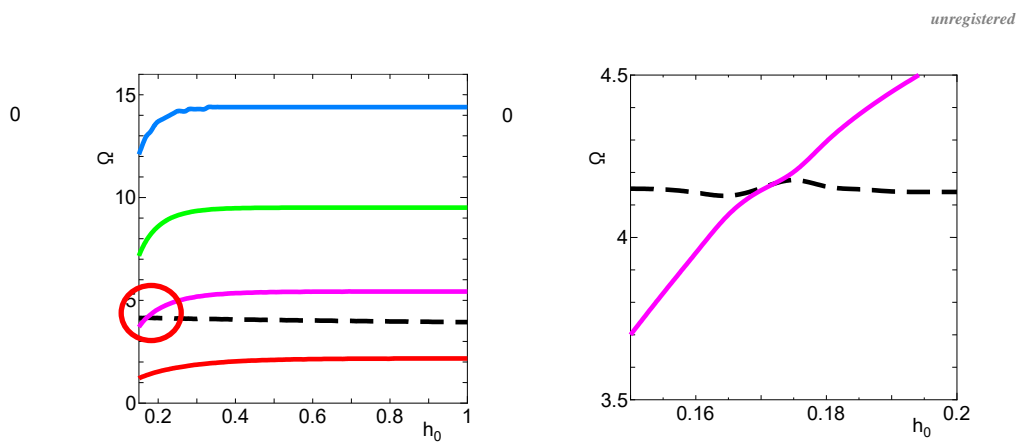
（ⅰ） Natural circular frequency curves. （ⅱ） Magnified view.

Fig. 13(a) Variation of coupled natural circular frequency with liquid height h_0 $(\theta_0 = 60^\circ, \bar{\rho} = 1,$

$\gamma = 1 \times 10^{-4}, \lambda = 10, \bar{\beta} = 10, \bar{m}_t = 1)$.; (i) Natural circular frequency curves.; (ii) Magnified view.
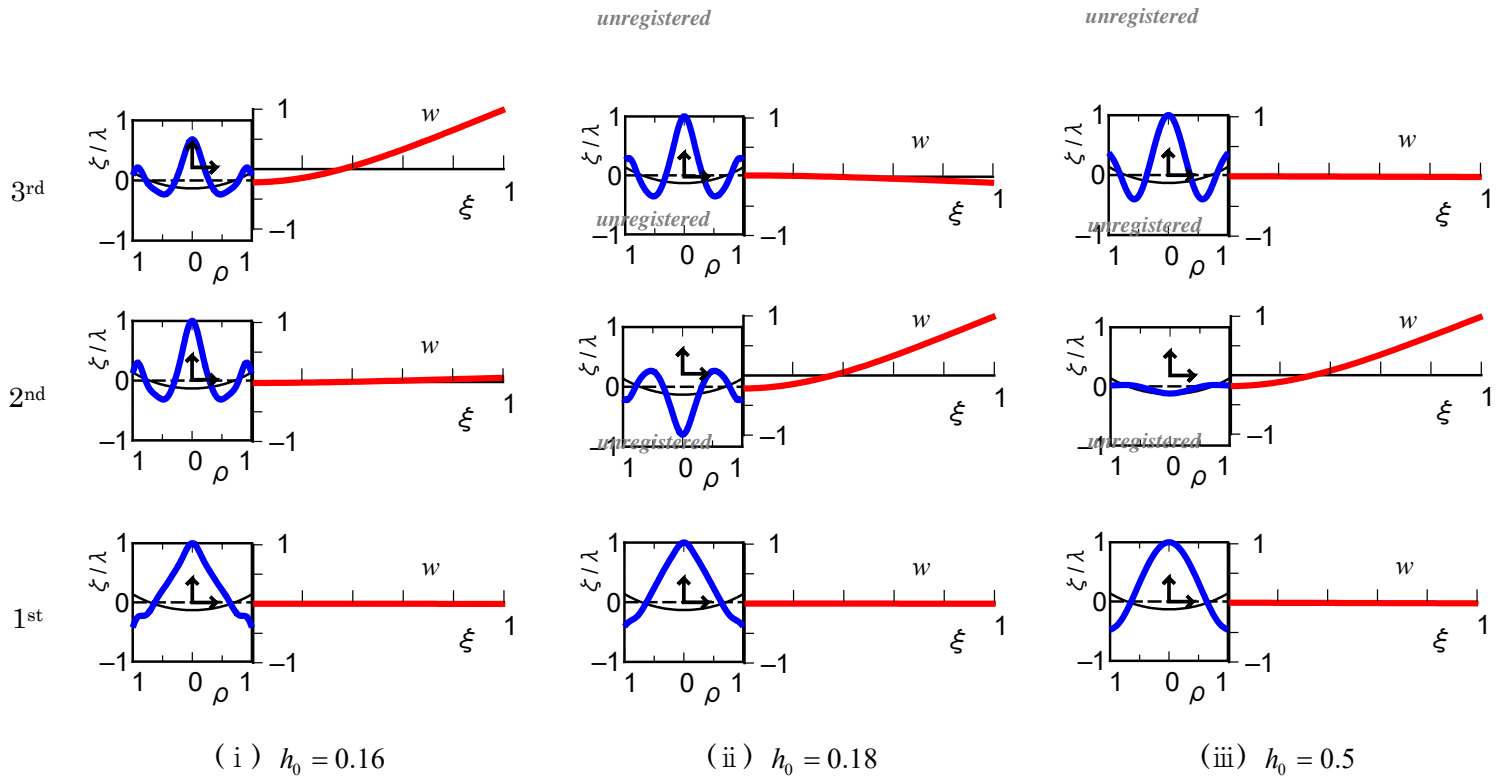
13
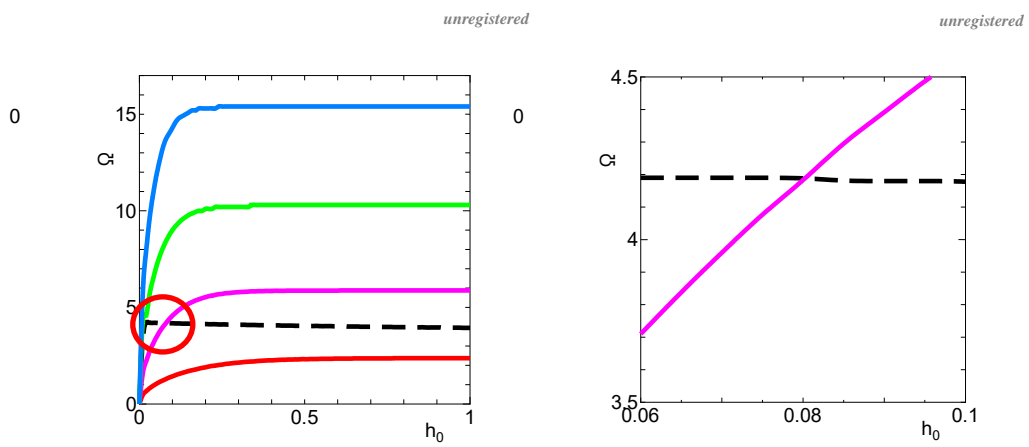
（ⅰ）　Natural circular frequency curves.　　　（ⅱ）　Magnified view.

Fig. 13(b) Variation of coupled natural circular frequency with liquid height h_0

$(\theta_0 = 90°, \bar{\rho} = 1,, \gamma = 1 \times 10^{-4}, \lambda = 10, \bar{\beta} = 10, \bar{m}_t = 1)$.;

(i) Natural circular frequency curves.; (ii) Magnified view.

14

(i) $h_0 = 0.16$ (ii) $h_0 = 0.18$ (iii) $h_0 = 0.5$

Fig. 14(a) Coupled vibration mode with liquid height

h_0 ($\theta_0 = 60°, \bar{\rho} = 1.0, \gamma = 1 \times 10^{-4}, \lambda = 10, \bar{\beta} = 10, , \bar{m}_t = 1$).; (i) $h_0 = 0.16$; (ii) $h_0 = 0.18$; (iii) $h_0 = 0.5$
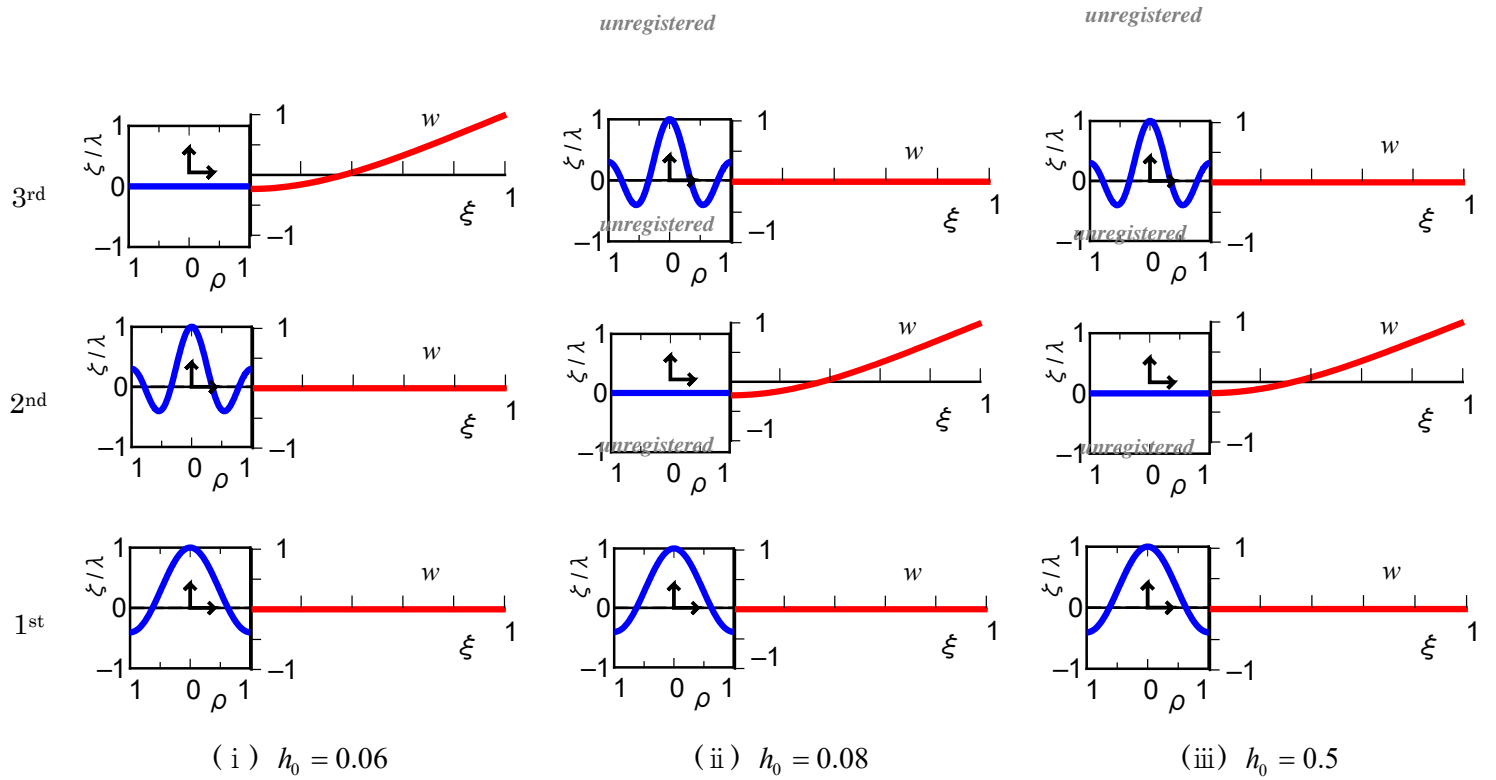
15

(ⅰ) $h_0 = 0.06$ (ⅱ) $h_0 = 0.08$ (ⅲ) $h_0 = 0.5$

Fig. 14(b) Coupled vibration mode with liquid height h_0 $(\theta_0 = 90^\circ, \bar{\rho} = 1.0, \gamma = 1 \times 10^{-6}, \lambda = 10, \bar{\beta} = 10,$

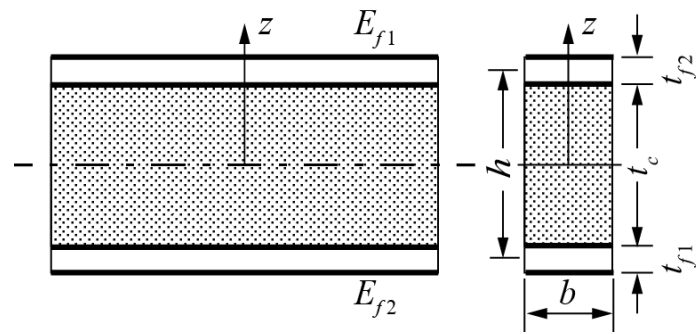$\bar{m}_t = 1$).; (i) $h_0 = 0.06$; (ii) $h_0 = 0.08$; (iii) $h_0 = 0.5$

Fig. B1 Sandwich beam